SUPPLEMENTALLY INFORMATION

A convenient method to estimate glass transition temperature of small organic semiconductor materials

Youichi Tsuchiya,*[,a] Nozomi Nakamura,[a] Shunta Kakumachi,[a,b] Keiko Kusuhara,[a] Chin-Yiu Chan[a] and Chihaya Adachi*[,a,b,c]

[a] Center for Organic Photonics and Electronics Research (OPERA), Kyushu University, 744 Motooka, Nishi-ku, Fukuoka 819-0395, Japan.

[b] Department of Chemistry and Biochemistry, Kyushu University, Kyushu University, 744 Motooka, Nishi-ku, Fukuoka 819-0395, Japan.

[c] International Institute for Carbon Neutral Energy Research (WPI-I2CNER), Kyushu University, 744 Motooka, Nishi-ku, Fukuoka 819-0395, Japan.

E-mails:

tsuchiya@opera.kyushu-u.ac.jp,
adachi@cstf.kyushu-u.ac.jp

Contents:

1. Experimental details

The organic semiconductors were purchased or synthesized by previously reported methods, and their purity was confirmed by the LC-ESI-MS analysis system consisting of HPLC, Waters Alliance 2695 with 3100 Mass Detector (Waters, USA) by using InertSustain C18 (GL Science, Japan) with a tetrahydrofuran-acetonitrile mixed system. **Cz-TRZ**,[S1] **PPT**,[S2] **DPEPO**,[S3] **5CzTRZ**,[S4] **HDT-1**,[S5] **TrisCz-TRZ**,[S6,] and **PXZ-TRZ**[S7] were synthesized by ourselves with the reported methods. **CBP** (Angene International Limited), **TCTA** (TCI), **TPD** (TCI), **TPBi** (Suzhou Geao New Material Co., Ltd.), and **4CzIPN** (Chemicalsoft Co., Ltd.) were purchased and purified with sublimation in our laboratory. **mCP** (Changchun Tuo Cai Technology Co.,ltd.), **mCBP** (NARD INSTITUTE, LTD.), **PyD2Cz** (Lumtec), **TAPC** (Lumtec), **Tris-PCz** (OODA KASEI CO., LTD.), ***α*-NPD** (NIPPON STEEL Chemical & Material CO., LTD.), ***m*-MTDATA** (Lumtec), **T2T** (NARD INSTITUTE, LTD.), **DPPS** (Lumtec), **TmPyPB** (Lumtec), **SF3-TRZ** (NARD INSTITUTE, LTD.) were directly used as is with or without the purity check. The thermal analysis was performed with thermogravimetry-differential thermal analysis (TG-DTA 2400SA, BRUKER, Germany) and differential scanning calorimetry (DSC; DSC 204 F1, NETZCH, Germany). TG-DTA measurements were performed with the scan rate of 10 °C/min under N_2 atmosphere.

To measure T_g values by using DSC, it is necessary to melt the samples at the 1st heating process. Then, the sample is quickly cooled to around 0 °C (1st cooling), providing a glass state of samples. Next, we heat the sample again to find the T_g signal (2nd heating). In this time, we employ 10 and 20 °C/min as the heating and cooling rate, and 10 min as an interval time for the first heating and cooling. This long interval time is a waiting time for blending the two materials at the melting state; this is the origin of the name of the melt-blending method. It should be noted that the incubation temperature must be lower than T_{dec} of blend components. To obtain homogeneous blend glass, it is better to use the blend samples ground well by an agate mortar and the incubation time at a high temperature can be tuned. It is important to check the sample state after the measurement of 2nd cooling (same rate with 1st cooling); the sample formed clear glass without whitish-fog or not.

References:

S1) J. Xiao, X.-K. Liu, X.-X. Wang, C.-J. Zheng, and F. Li, *Org. Electron.* **2014**, 2763–2768.
S2) C. Fan, C. Duan, Y. Wei, D. Ding, H. Xu, and W. Huang, *Chem. Mater.* 2015, **27**, 5131–5140.
S3) J. Fawcett, A. W. G.Platt, S. Vickers, M. D.Ward, Polyhedron **2004**, 2561–2567.
S4) L.-S. Cui, A. J. Gillett, S.-F. Zhang, H. Ye, Y. Liu, X.-K. Chen, Z.-S. Lin, E. W. Evans, W. K. Myers, T. K. Ronson, H. Nakanotani, S. Reineke, J.-L. Bredas, C. Adachi, and R. H. Friend, *Nat. Photon.* 2020, **14**, 636–642.
S5) C.-Y. Chan, M. Tanaka, Y.-T. Lee, Y.-W. Wong, H. Nakanotani, T. Hatakeyama, and C. Adachi, *Nat. Photon.* 2021, **15**, 203–207.
S6) S. Hirata, Y. Sakai, K. Masui, H. Tanaka, S.-Y. Lee, H. Nomura, N. Nakamura, M. Yasumatsu, H. Nakanotani, Q. Zhang, K. Shizu, H. Miyazaki, and C. Adachi, Nat. Materials 2015, **14**, 330–336.
S7) H. Tanaka, K. Shizu, H. Miyazaki, C. Adachi, Chem Commun. 2012, **48**, 11392–11394.

2. Structures of Materials

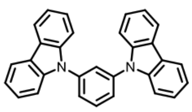
mCP

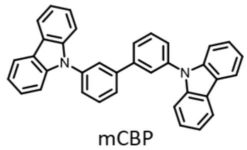
mCBP

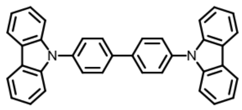
CBP

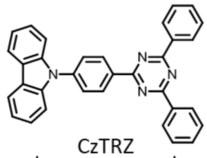
CzTRZ

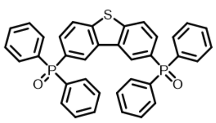
PPT

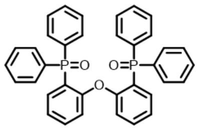
DPEPO

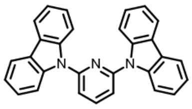
Py2DCz

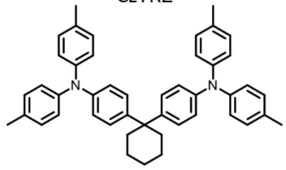
TAPC

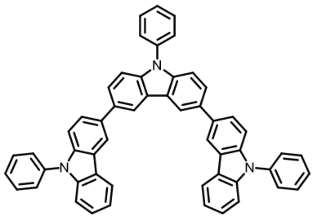
Tris-PCz

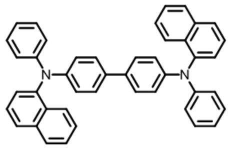
α-NPD

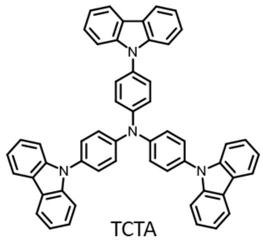
TCTA

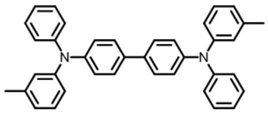
TPD

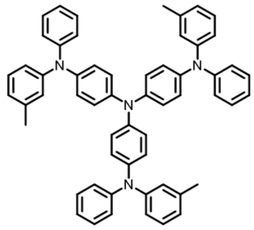
m-MTDATA

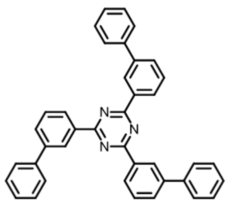
T2T

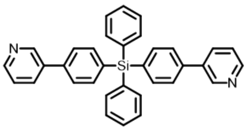
DPPS

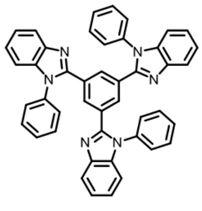
TPBi

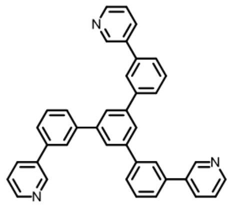
TmPyPB

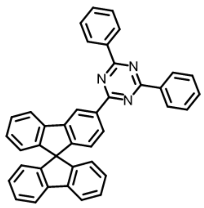
SF3-TRZ

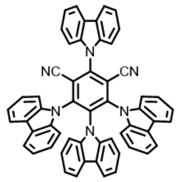
4CzIPN

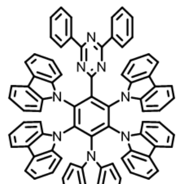
5CzTRZ

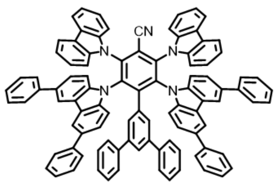
HDT-1

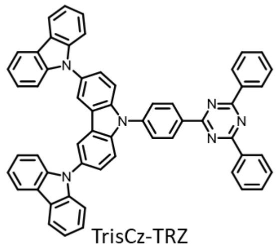
TrisCz-TRZ

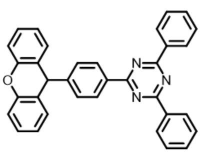
PXZ-TRZ

3. Derivation of Fox equation

In general, T_g (in Kelvin) of amorphous polymer blends between two components, A and B, follows the relationship of the Gordon-Taylor equation with T_g of each component ($T_{g,A}^0$ and $T_{g,B}^0$).[8]

$$T_g = \frac{w_A T_{g,A}^0 + k w_B T_{g,B}^0}{w_A + k w_B} = \frac{(1 - w_B) T_{g,A}^0 + k w_B T_{g,B}^0}{(1 - w_B) + k w_B}, \tag{S3.1}$$

where w_A and w_B are the weight fraction of each component A and B. k is the ratio related to the T_g values and densities of the glass states (ρ_A^0 and ρ_B^0) for each component as follows,[9]

$$k = \frac{T_{g,A}^0}{T_{g,B}^0} \cdot \frac{\rho_A^0}{\rho_B^0}. \tag{S3.2}$$

When $\rho_A^0 = \rho_B^0$ is employed as the assumption, the equation can be rewritten as the simple form called Fox equation as follows,[7]

$$\frac{1}{T_g} = \frac{w_A}{T_{g,A}^0} + \frac{w_B}{T_{g,B}^0} = \frac{1 - w_B}{T_{g,A}^0} + \frac{w_B}{T_{g,B}^0}. \tag{S3.3}$$

4. Coefficient of determination, R^2

Eqn (4) derived from the Fox equation does not give an exact liner relationship between the theoretical T_g and the fraction of the target compound but it gives an approximately linear relationship. In this report, therefore, the most general R^2 which is defined by the residual sum of squares (RSS) and a total sum of squares (TSS) was employed as an accuracy value for theoretically estimated T_g.

$$R^2 = 1 - \frac{RSS}{TSS} = 1 - \frac{\sum_{i=1}^{n} (y_i - \widehat{y_i})^2}{\sum_{i=1}^{n} (y_i - \overline{y_i})^2}, \tag{S4.1}$$

where y_i are the set of observations, $\widehat{y_i}$ is the set of theocraticals, and $\overline{y_i}$ is the average of y_i. The R^2 value is sometimes provided as a negative value, which means the theoretical model cannot explain the observed values.

5. Note for plots of T_g versus fraction of blends

The Fox equation does not provide the liner plot for T_g of blends. When it is required the pictures in the exact liner relationship, the deformed eqns (S5.2) and (S5.3) can be employed to draw the theoretical line and plot the observed T_g instead of eqn (4).

$$T_g = T_{g,matrix}^0 T_{g,target}^0 W \tag{S5.2}$$

$$W = \frac{1}{T_{g,target}^0 + \left(T_{g,matrix}^0 - T_{g,target}^0\right) w_{target}} \tag{S5.3}$$

where $T_{g,target}^0$ is the average estimated T_g value for the target material from each observed T_g value. It should note that Kelvin was used as the temperature to apply each equation while those values were written in the Celsius degree in the main text, Figures, and Tables.

6. Full scaled DSC thermal profile of organic semiconductor blends

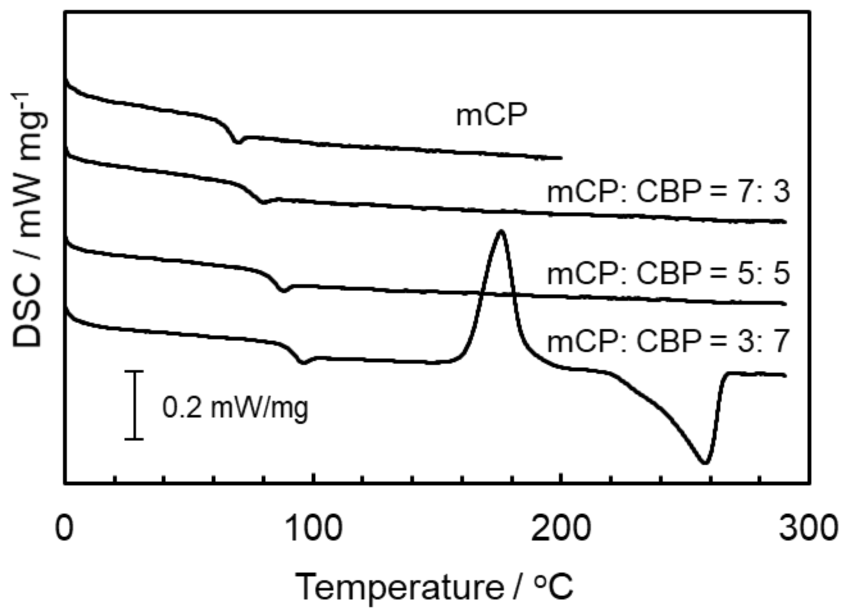

Fig. S1 DSC curves of **mCP**/**CBP** blends with the various blend ratio at 2nd heating.

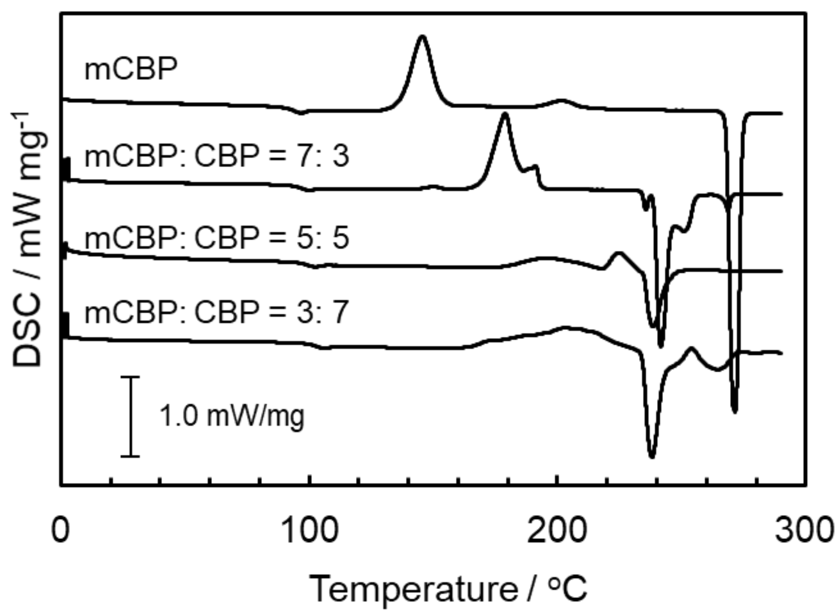

Fig. S2 DSC curves of **mCBP**/**CBP** blends with the various blend ratio at 2nd heating.

7. DSC thermal profile and T_g analysis of T2T blends

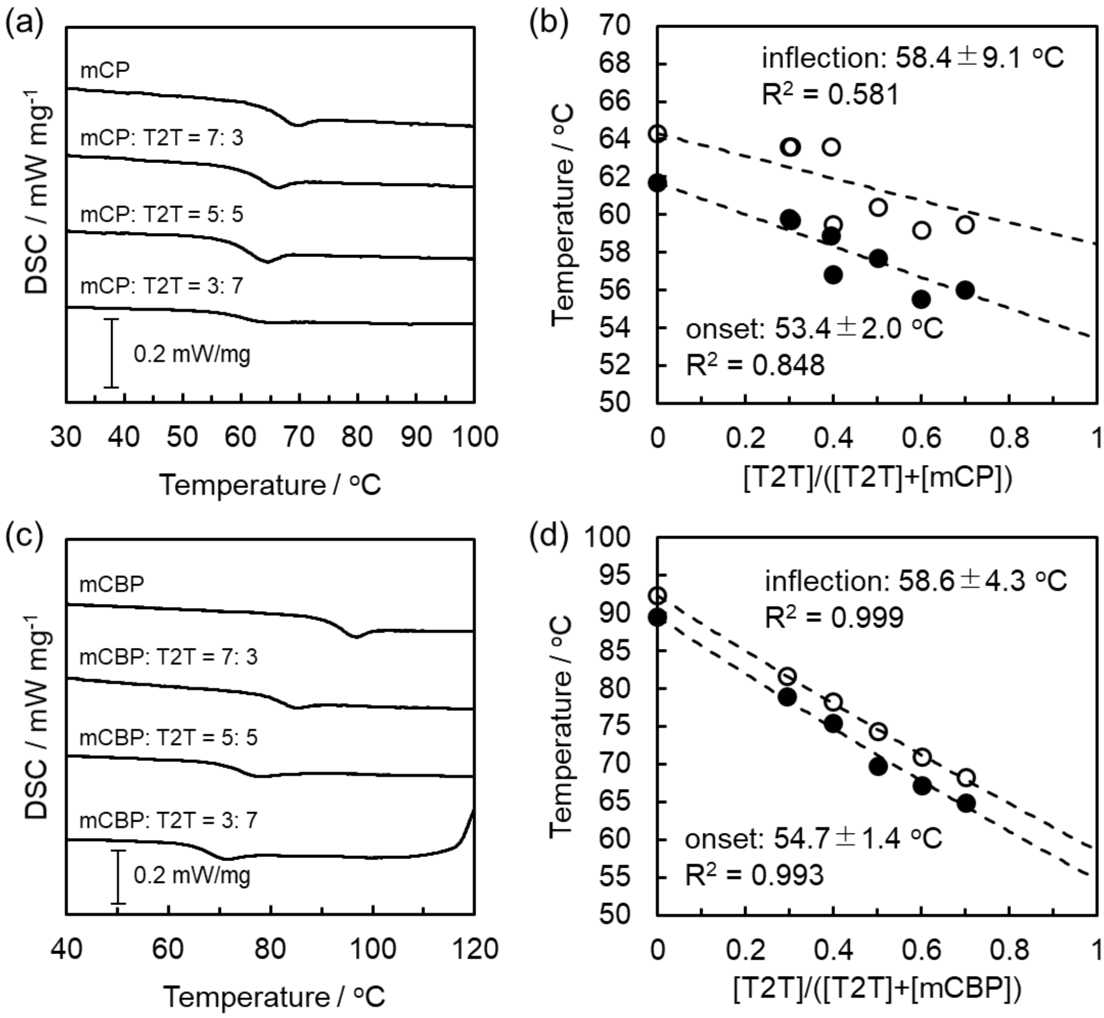

Fig. S3 (a and c) T_g signals of **T2T** blends at second heating of DSC measurement with **mCP** (a) or **mCBP** (c) as a matrix. (b and d) Plots of inflection (open circle) and onset T_g values (closed circle) versus CBP fraction of each blend; (b) **mCP** and (d) **mCBP**. Broken lines were obtained with eqn (4) as theoretical curve of the Fox equation.

8. Full scaled DSC thermal profile of T2T blends

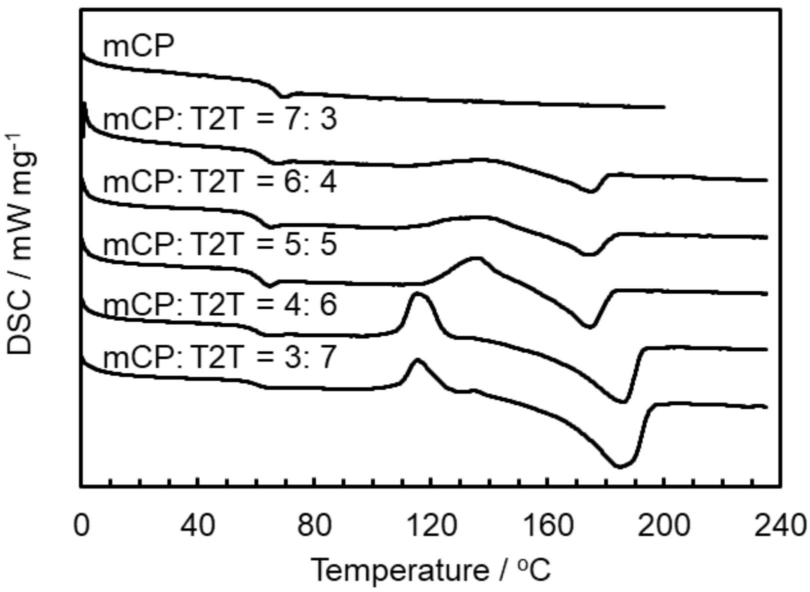

Fig. S4 DSC curves of **mCP**/**T2T** blends with the various blend ratio at 2nd heating.

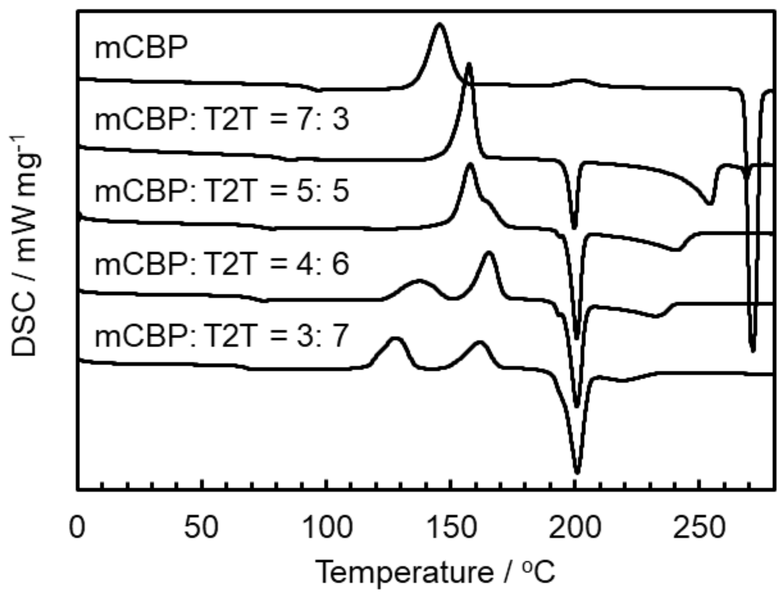

Fig. S5 DSC curves of **mCBP**/**T2T** blends with the various blend ratio at 2nd heating.

9. DSC analysis of T2T with quick cooling by liquid N_2

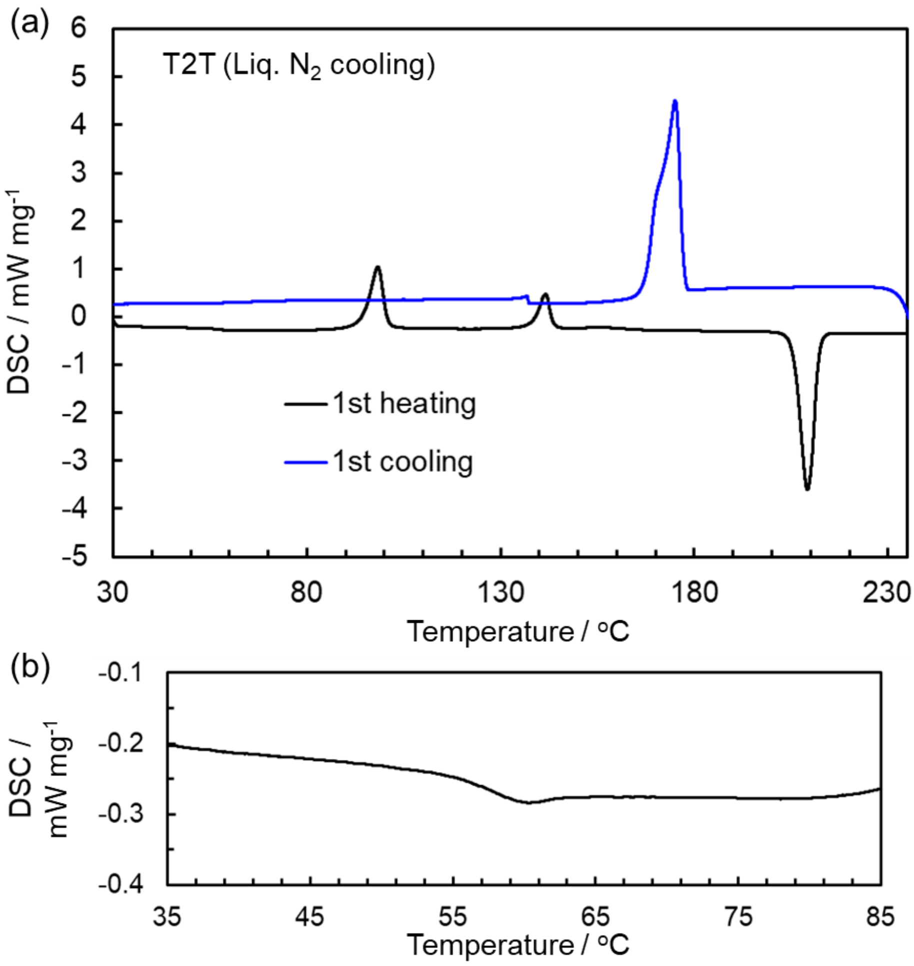

Fig. S6 (a) DSC curves of **T2T** by heating and cooling processes. (b) Focusing T_g signal at 1st heating. The sample **T2T** in an aluminum pan was cooled into liquid N_2 after heating to 230 °C on hot plate.

10. Results of T_g estimation using melt-blending methods for 4CzIPN and 5CzTRZ

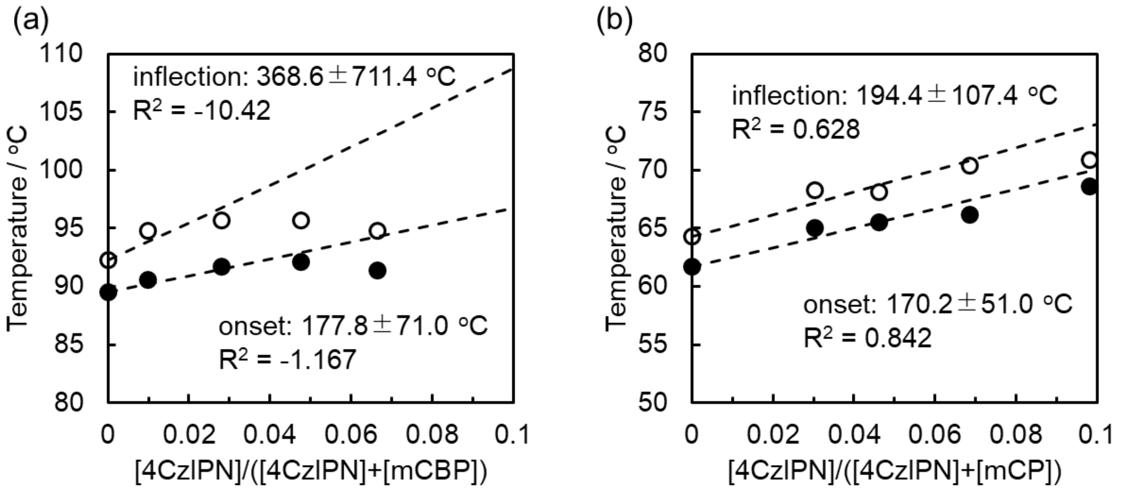

Fig. S7 Plots of inflection (open circle) and onset T_g values (closed circle) versus **4CzIPN** fraction of **4CzIPN**-**mCBP** (a) or **4CzIPN**-**mCP** (b) blends; the horizontal scale was emphasized from 0 to 0.1. Broken lines were obtained with eqn (4) as theoretical curve of Fox equation.

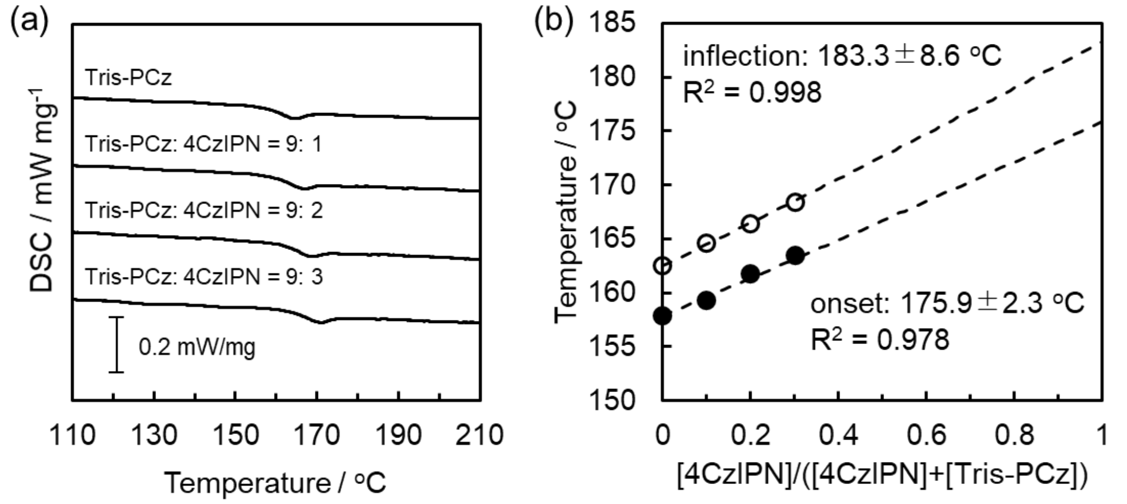

Fig. S8 (a) T_g signals of **4CzIPN** blends at second heating of DSC measurement with **Tris-PCz** as a matrix. (b) Plots of inflection (open circle) and onset T_g values (closed circle) versus **4CzIPN** fraction of each blend. Broken lines were obtained with eqn (4) as theoretical curve of Fox equation.

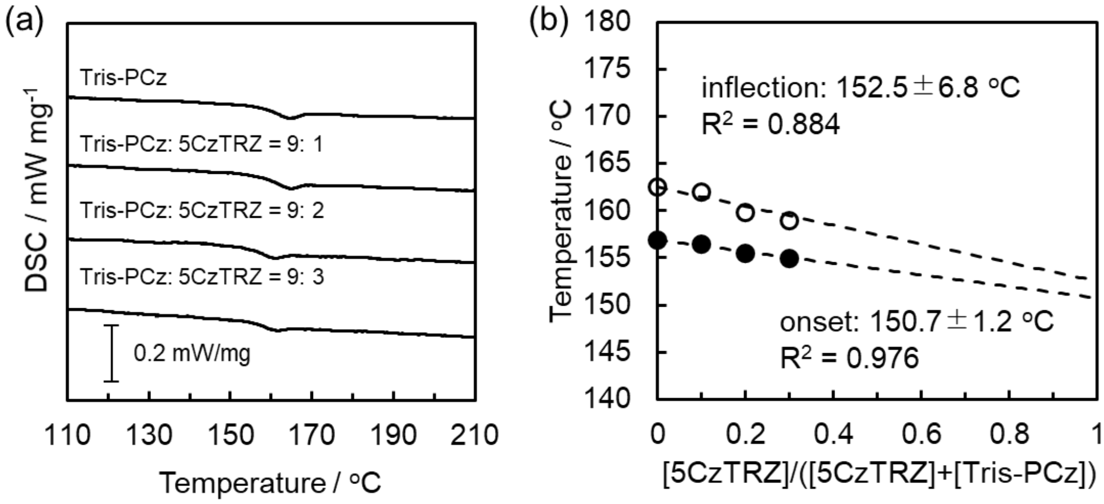

Fig. S9 (a) T_g signals of **5CzTRZ** blends at second heating of DSC measurement with **Tris-PCz** as a matrix. (b) Plots of inflection (open circle) and onset T_g values (closed circle) versus **5CzTRZ** fraction of each blend. Broken lines were obtained with eqn (4) as theoretical curve of Fox equation.

11. Summary of Thermal behavior of organic semiconductors

Table S1. Thermo-physical parameters for interest OLED materials (cooling rate, 20 °C min^{-1}; heating rate, 10 °C/ min)

	Purity	T_g^i/ °C	T_g^o/ °C	T_c/ °C	T_m[f)]/ °C	T_{dec}[g)]/ °C	T_g^{Lit}/ °C
				Host materials			
mCP	1.000	64	62	N.D.	177	-	55 (-/-/-)[S8], 60 (-/-/-)[S9], 65 (100/10/i)[S10], 66 (-/-/-)[S11]
mCBP	0.999	92	90	137	271	349	92 (100/10/i)[S10], (-/-/-)[S11]
CBP	0.996	109	103	162[b)]	282	-	62 (-/-/-)[S9], 112(Liq.N_2/50/i)[S12]
Cz-TRZ	0.999	92	90	149	276	345	N/A
PPT	0.999	109	105	N.D.	252	406	107 (-/-/-)[S11]
DPEPO	0.994	95	90	160	282	316	93 (100/10/i)[S10], 94 (-/-/-)[S11]
PyD2Cz	> 0.99[a)]	74	70	N.D.	308	319	N/A
				Hole transporting materials			
TAPC	0.996	86	82	N.D.	187	357	78 (10/10/-)[S13], 79 (-/-/-)[S14], 89 (-/-/-)[S15]
Tris-PCz	0.999	163	157	N.D.	N.D.	481	154 (100/10/i)[S10]
α-NPD	0.998	101	95	211	282	375	75 (-/-/-)[S16], 95 (-/-/-)[S17], 96 (-/-/-)[S14], 99 (-/-/-)[S11] 100 (-/-/-)[S15]
TCTA	0.997	155	152	N.D.	300	471	151 (-/5/o)[S18], (-/-/-)[S19]
TPD	0.997	65	63	N.D.	171	329	58 (-/-/-)[S14], 60 (10/10/-)[S20], (-/5/-)[S11], (-/-/-)[S18], 61 (-/-/-)[S16], 63 (-/-/-)[S21], 65 (10/10/-)[S22]
m-MTDATA	> 0.99[a)]	82	76	N.D.	206	399	75 (-/-/-)[S14], (-/-/o)[S23]
				Electron transporting materials			
T2T	1.000	59 56[c)]	55 55[c)]	109[b)] 94[c)]	214	366	55 (-/-/-)[S24], 95 (-/-/-)[S25]
DPPS	> 0.99[a)]	53	50	N.D.	154	312	N/A
TPBi	0.999	123	120	N.D.	277	381	122 (-/-/-)[S26], 124 (-/-/i)[S27], 127 (-/10/-)[S28]
TmPyPB	0.993	79	76	121[d)]	198	395	79 (-/10/-)[S29]
SF3-TRZ	1.000	134	130	207	278	348	135 (-/-/i)[S30]
				TADF materials			
4CzIPN	0.993	183	176	265[e)]	381	389	N/A
5CzTRZ	0.994	153	151	N.D.	471	486	N/A
HDT-1	0.999	205	197	N.D.	414	491	N/A
TrisCz-TRZ	0.998	198	195	N.D.	354	491	197 (-/10/-)[S31]
PXZ-TRZ	0.995	89	87	138	308	351	N/A

All values were written by considering the number of significant figures. a) Information from vendor company. b) Estimated from **mCP** blend with the fraction of 0.7. c) Using sample cooled with liquid N_2 after heating T_m+20 °C on heater at air atmosphere condition. d) Estimated from first heating of DSC. e) Estimated from **Tris-PCz** blend with the fraction of 0.3. f) peak value in DTA measurement. g) 0.5% weight loss in TG measurement. h) indicating in parentheses as cooling rate (°C/min)/ heating rate (°C/min)/ inflection (i) or onset (o); "-" means not provided.

References for Table S1:

S8) S.-J. Yeh, M.-F. Wu, C.-T. Chen, Y.-H. Song, Y. Chi, M.-H. Ho, S.-F. Hsu and C.-H. Chen, *Adv. Mater.* 2005, **17**, 285-289.

S9) M.-H. Tsai, Y.-H. Hong, C.-H. Chang, H.-C. Su, C.-C. Wu, A. Matoliukstyte, J. Simokaitiene, S. Grigalevicius, J. V. Grazulevicius and C.-P. Hsu, *Adv. Mater.* 2007, **19**, 862. (= Ref. 11)

S10) B. A. Naqvi, M. Schmid, E. Crovini, P. Sahay, T. Naujoks, F. Rodella, Z. Zhang, P. Strohriegl, S. Bräse, E. Zysman-Colman and W. Brütting, *Front. Chem.* 2020, **8**, 750.

S11) N. Notsuka, R. Kabe, K. Goushi and C. Adachi, *Adv. Funct. Mater.* 2017, **27**, 1703902.

S12) N. Van den Brande, A. Gujral, C. Huang, K. Bagchi, H. Hofstetter, L. Yu, and M. D. Ediger, *Cryst. Growth Des.* 2018, **18**, 5800‑5807. (= Ref. 12)

S13) P. Strohrigl and J. V. Grazulevicius, *Adv. Mater.* 2002, **14**, 1439-1452.

S14) M. Aonuma, T. Oyamada, H. Sasabe, T. Miki, C. Adachi, *Appl. Phys. Lett.* 2007, **90**, 183503.

S15) Shahnawaz, S. S. Swayamprabha, M. R. Nagar, R. A. K. Yadav, S. Gull, D. K. Dubey and J.-H. Jou, *J. Mater. Chem. C* 2019, **7**, 7144–7158.

S16) Y. Shirota, K. Okumoto and H. Inada, *Synth. Metals* 2000, **111–112**, 387–391.

S17) S. A. Van Slyke, C. H. Chen, and C. W. Tang, *Appl. Phys. Lett.* 1996, **69**, 2160-2162.

S18) K. Naito and A. Miura, *J. Phys. Chem.* 1993, **97**, 6240–6248.

S19) Y. Kuwabara, H. Ogawa, H. Inada, N. Noma and Y. Shirota, *Adv. Mater.* 1994, **6**, 677–679.

S20) H. Tanaka, S. Tokito, Y. Taga and A. Okada, *J. Chem. Soc., Chem. Commun.* 1996, 2175–2176.

S21) D. M. Pai, J. F. Yanus and M. Stolka, *J. Phys. Chem.* 1984, **88**, 4714–4717.

S22) P. Strohrigl and J. V. Grazulevicius, *Adv. Mater.* 2002, **14**, 1439-1452.

S23) Y. Shirota, T. Kobata and N. Noma, *Chem. Lett.* 1989, **18**, 1145–1148.

S24) D. P. K. Tsang and C. Adachi, *Sci. Rep.* 2016, **6**, 22463. (= Ref. 18)

S25) H.-F. Chen, S.-J. Yang, Z.-H. Tsai, W.-Y. Hung, T.-C. Wang and K.-T. Wong, *J. Mater. Chem.* 2009, **19**, 8112. (= Ref 17)

S26) C. Mayr and W. Brütting, *Chem. Mater.* 2015, **27**, 2759–2762.

S27) H. K. Kim , Y. H. Byun , R. R. Das , B. K. Choi and P. S. Ahn, *Appl. Phys. Lett.* 2007, **91**, 093512.

S28) Z. Wang, P. Lu, S. Chen, Z. Gao, F. Shen, W. Zhang, Y. Xu, H. S. Kwok and Y. Ma, *J. Mater. Chem.* 2011, **21**, 5451-5456.

S29) S.-J. Su, Y. Takahashi, T. Chiba, T. Takeda and J. Kido, Adv. *Funct. Mater.* 2009, **19**, 1260.

S30) L.-S. Cui, S.-B. Ruan, F. Bencheikh, R. Nagata, L. Zhang, K. Inada, H. Nakanotani, L.-S. Liao and C. Adachi, *Nat. Commun.* 2017, **8**, 2250.

S31) Y. Li, J.-J. Liang, H.-C. Li, L.-S. Cui, M.-K. Fung, S. Barlow, S. R. Marder, C. Adachi, Z.-Q. Jiang and L.-S. Liao, *J. Mater. Chem. C* 2018, **6**, 5536–5541.

12. DSC data for bulk organic semiconductors

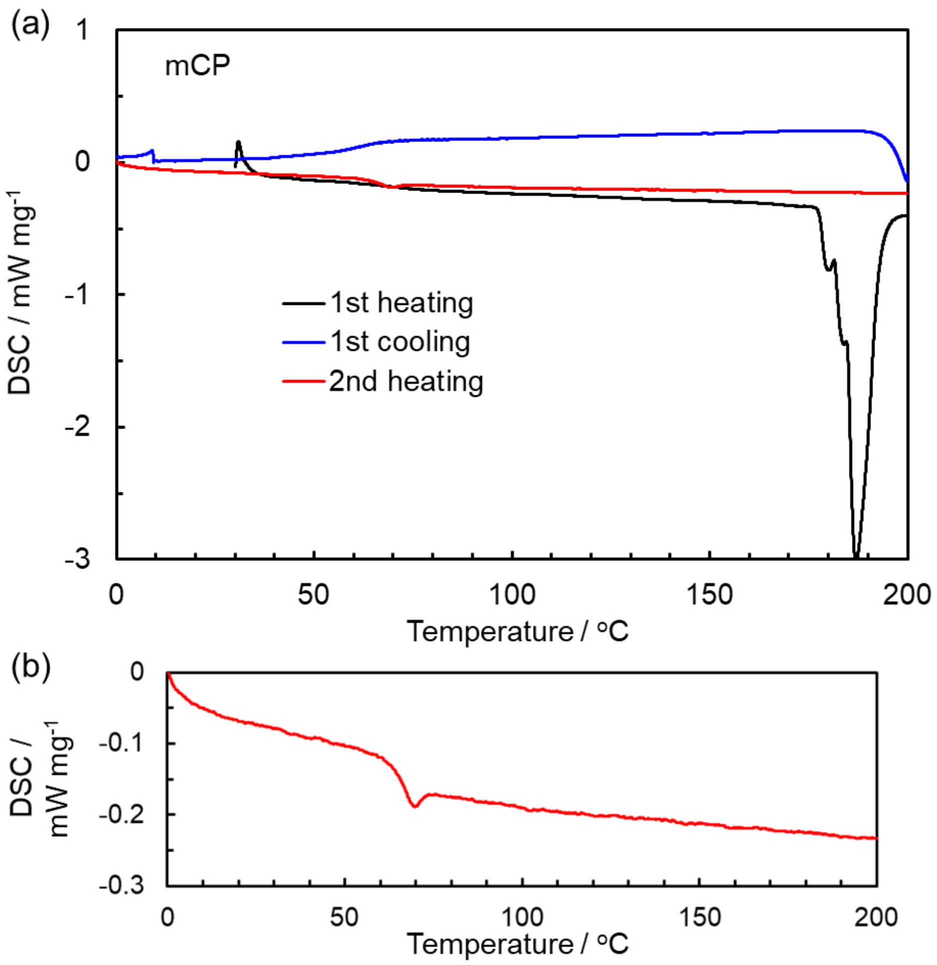

Fig. S10 (a) DSC curves of **mCP** by heating and cooling processes. (b) Focusing T_g signal at 2nd heating.

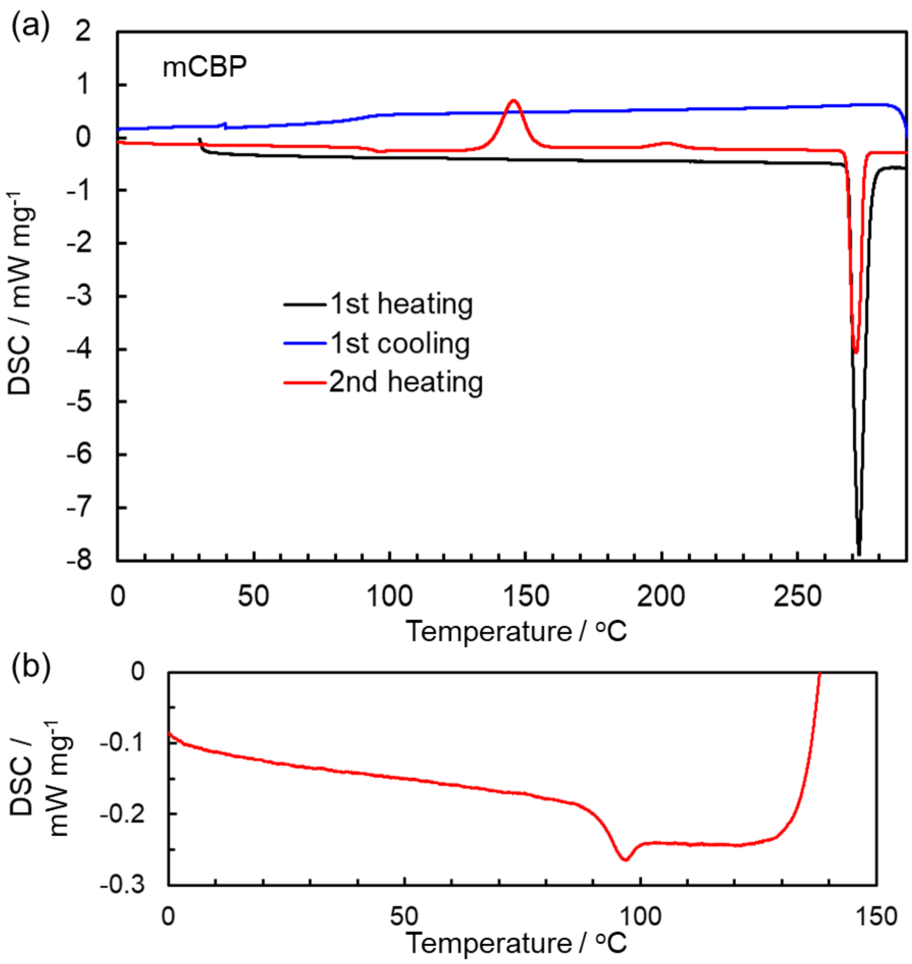

Fig. S11 (a) DSC curves of **mCBP** by heating and cooling processes. (b) Focusing T_g signal at 2nd heating.

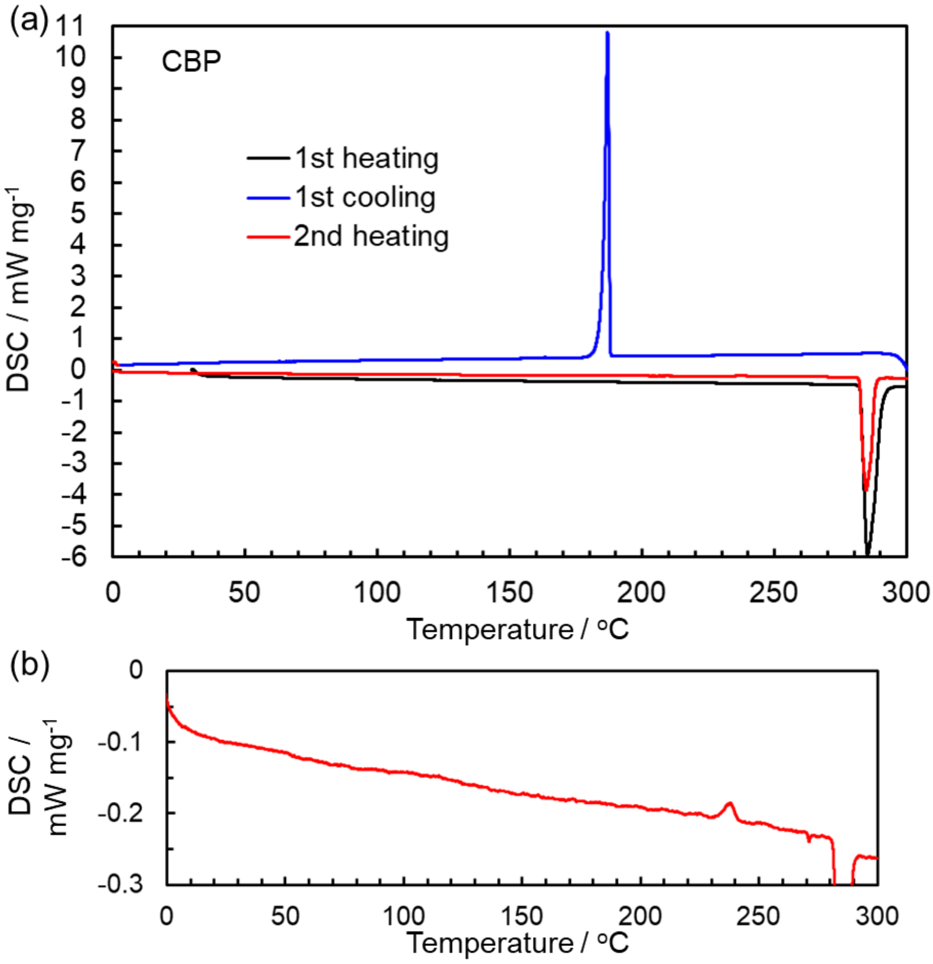

Fig. S12 (a) DSC curves of **CBP** by heating and cooling processes. (b) Focusing T_g signal at 2nd heating.

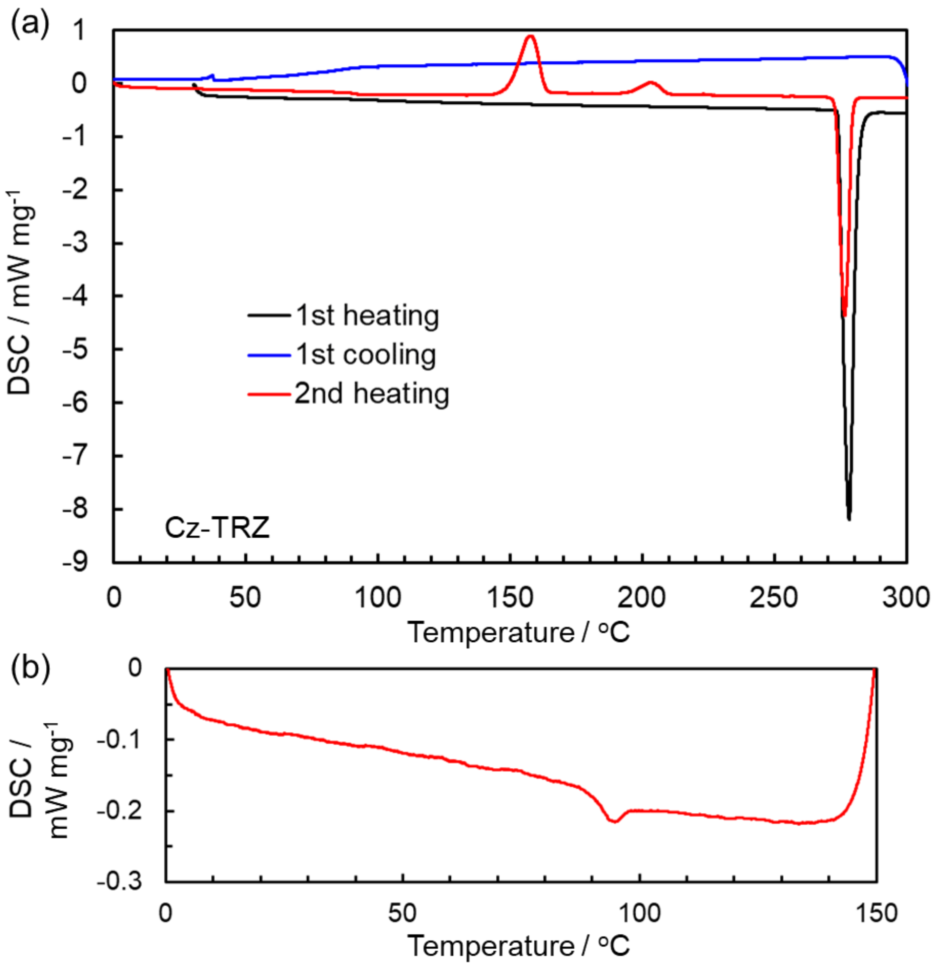

Fig. S13 (a) DSC curves of **Cz-TRZ** by heating and cooling processes. (b) Focusing T_g signal at 2nd heating.

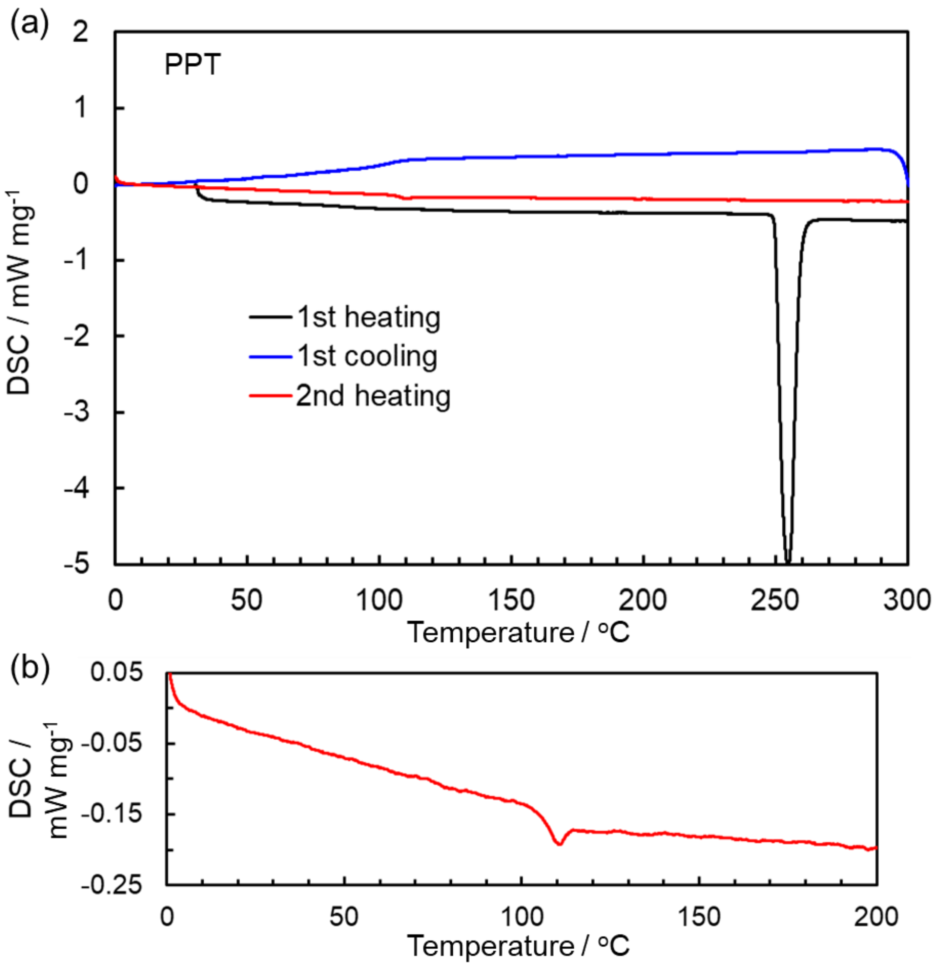

Fig. S14 (a) DSC curves of **PPT** by heating and cooling processes. (b) Focusing T_g signal at 2nd heating.

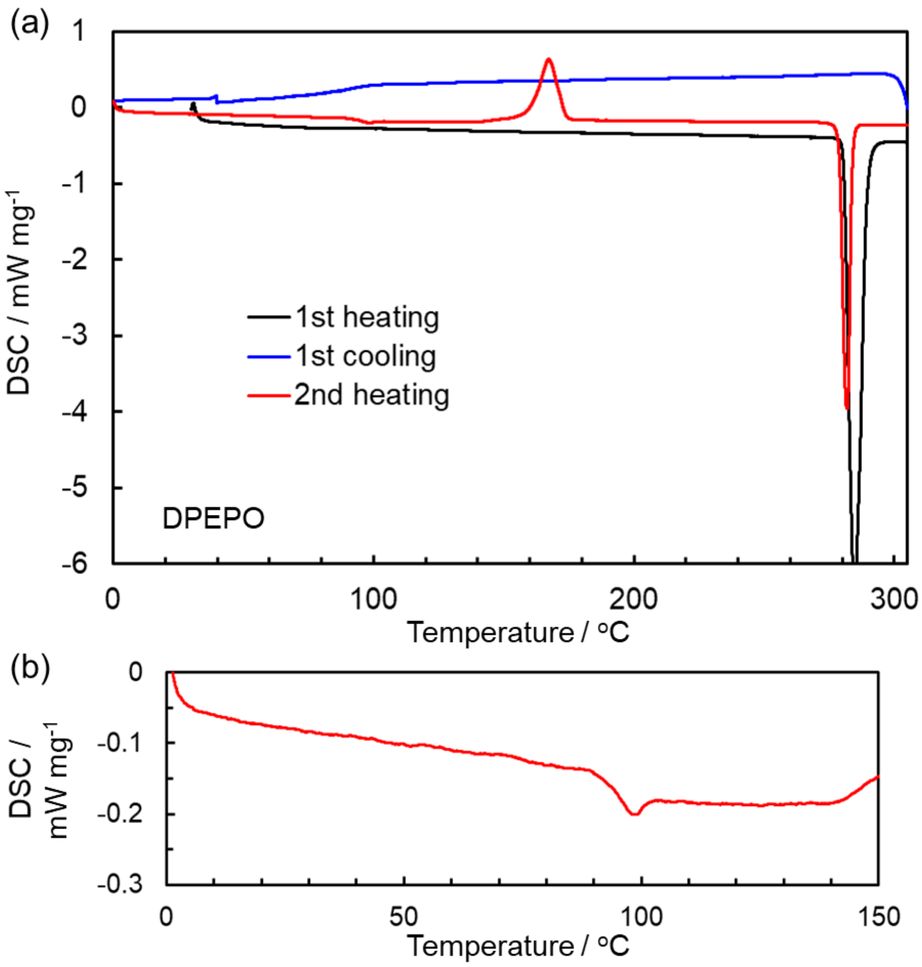

Fig. S15 (a) DSC curves of **DPEPO** by heating and cooling processes. (b) Focusing T_g signal at 2[nd] heating.

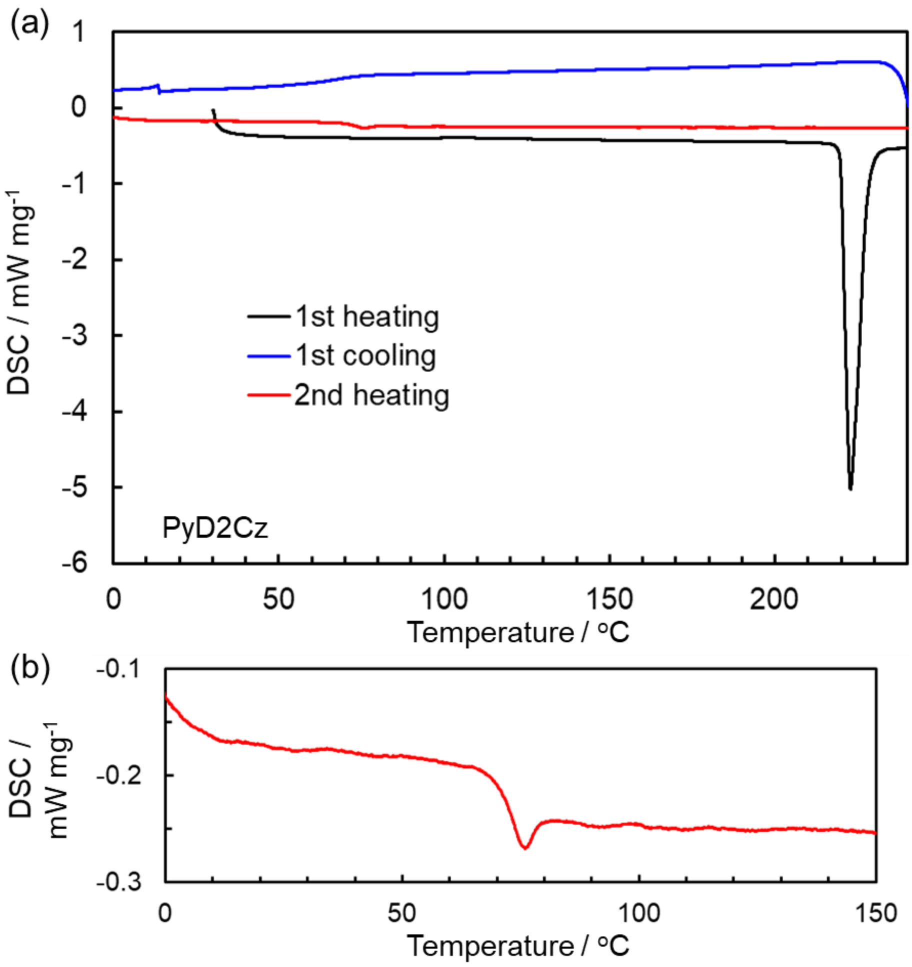

Fig. S16 (a) DSC curves of **PyD2Cz** by heating and cooling processes. (b) Focusing T_g signal at 2nd heating.

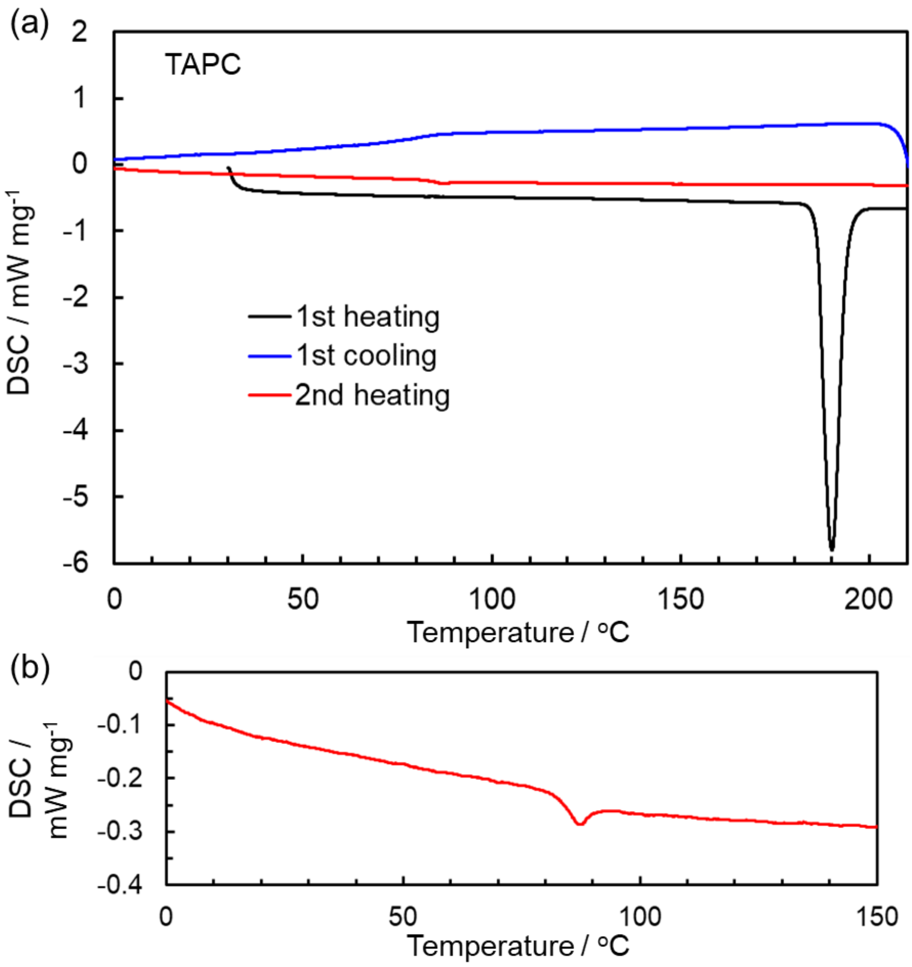

Fig. S17 (a) DSC curves of **TAPC** by heating and cooling processes. (b) Focusing T_g signal at 2nd heating.

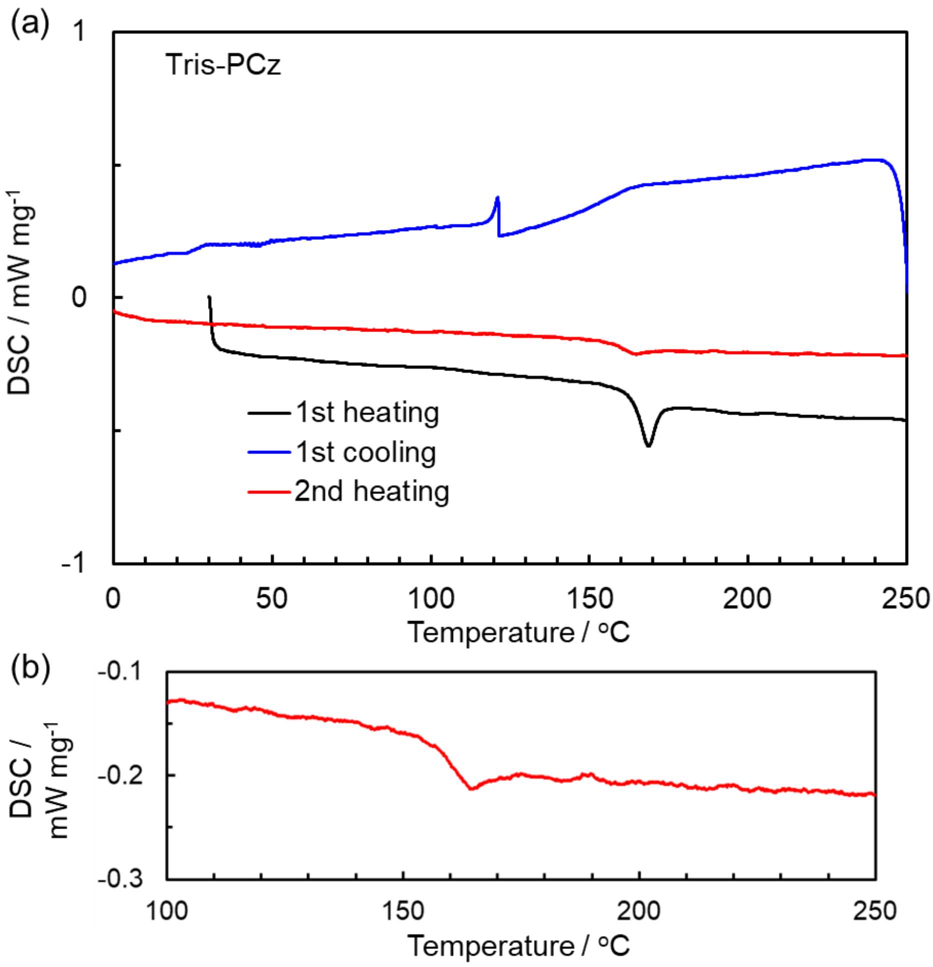

Fig. S18 (a) DSC curves of **Tris-PCz** by heating and cooling processes. (b) Focusing T_g signal at 2nd heating.

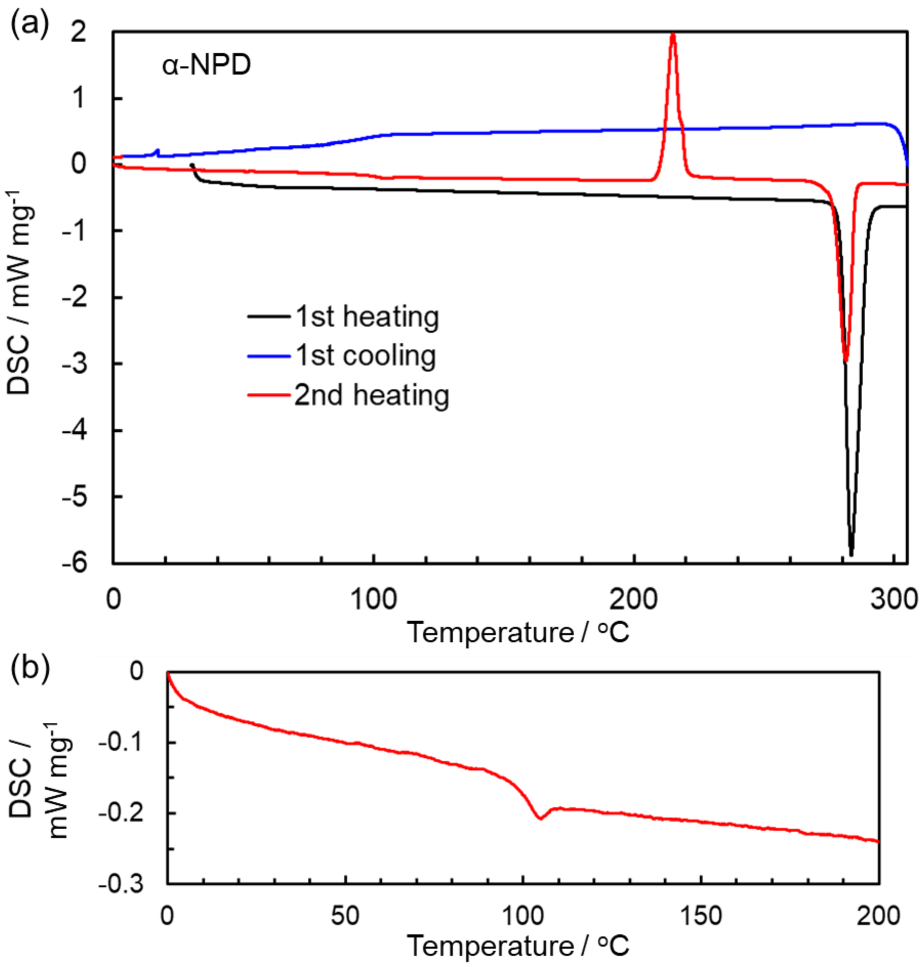

Fig. S19 (a) DSC curves of **α-NPD** by heating and cooling processes. (b) Focusing T_g signal at 2[nd] heating.

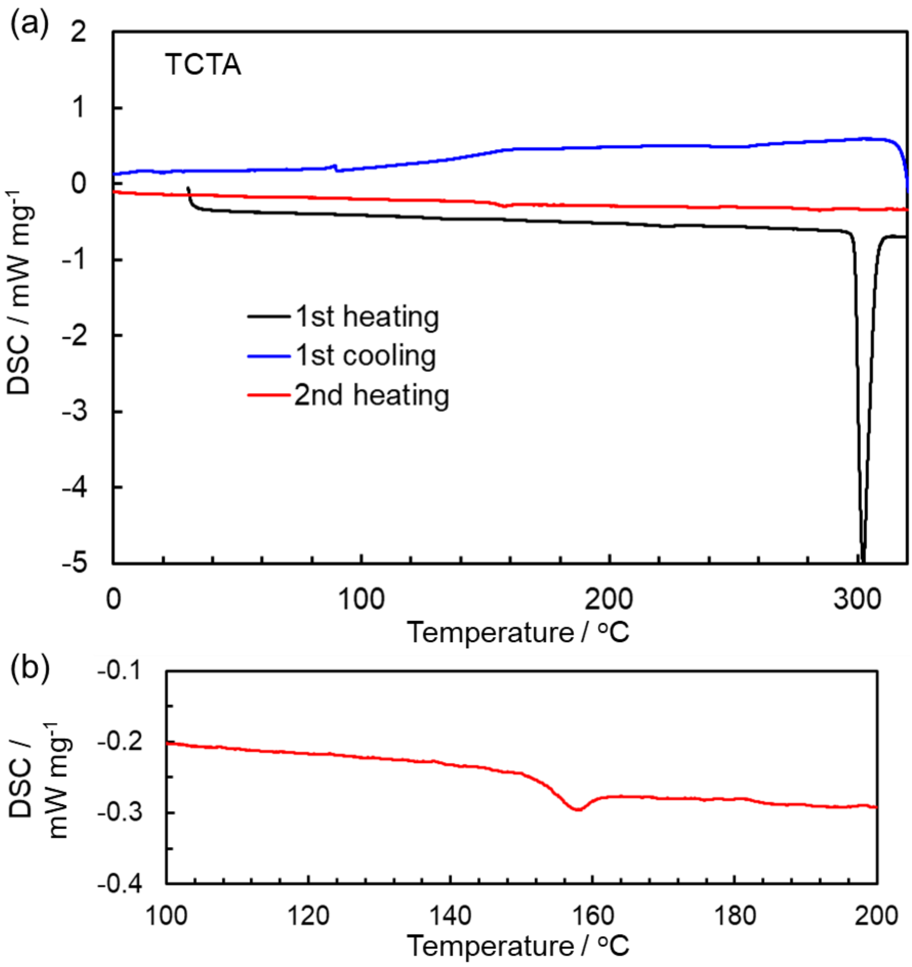

Fig. S20 (a) DSC curves of **TCTA** by heating and cooling processes. (b) Focusing T_g signal at 2nd heating.

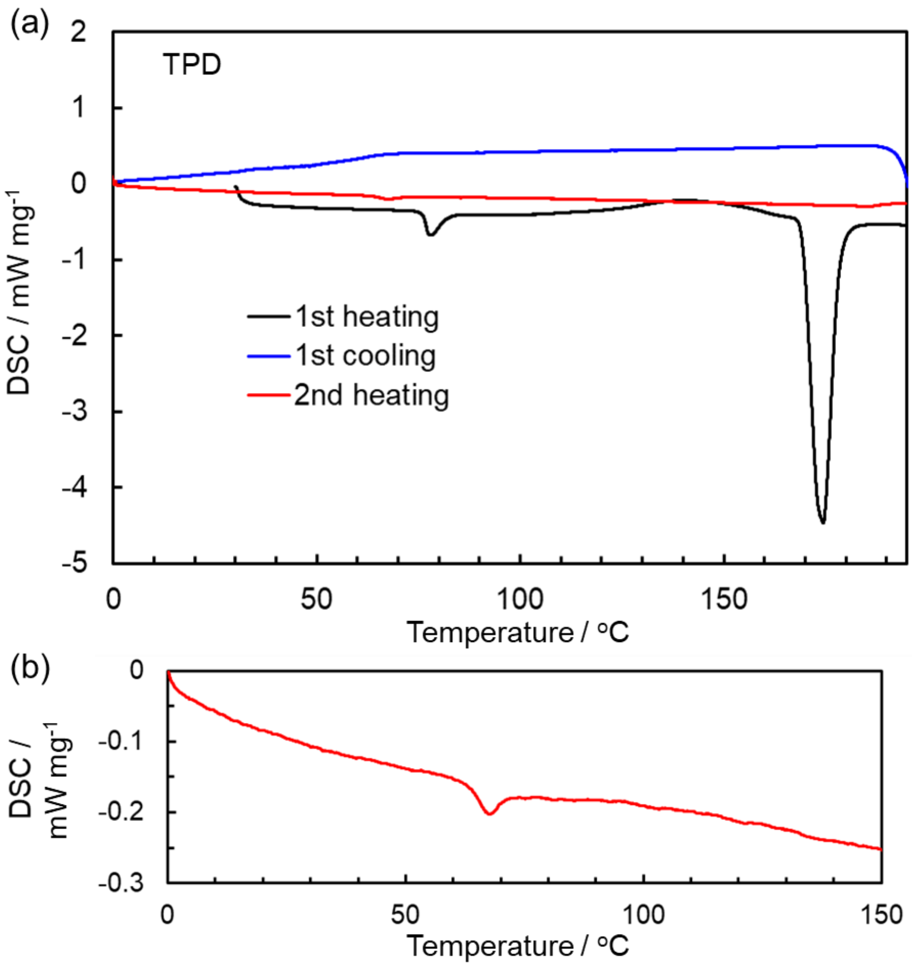

Fig. S2! (a) DSC curves of **TPD** by heating and cooling processes. (b) Focusing T_g signal at 2nd heating.

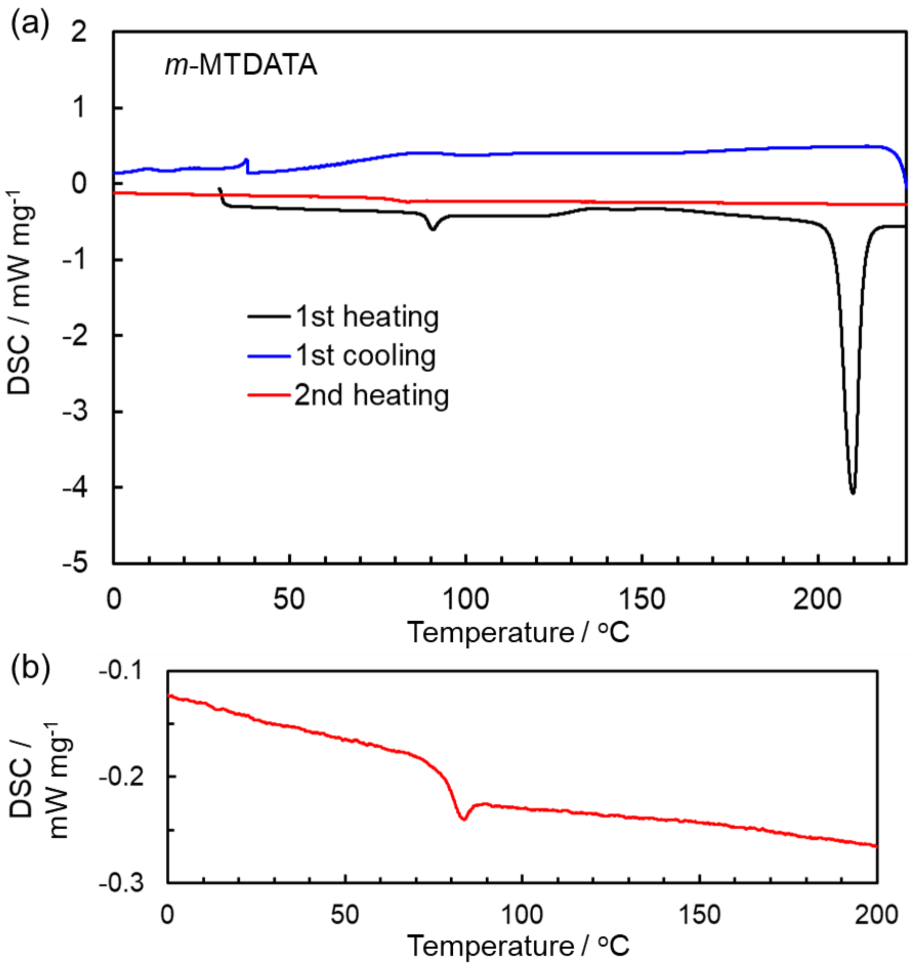

Fig. S22 (a) DSC curves of ***m*-MTDATA** by heating and cooling processes. (b) Focusing T_g signal at 2[nd] heating.

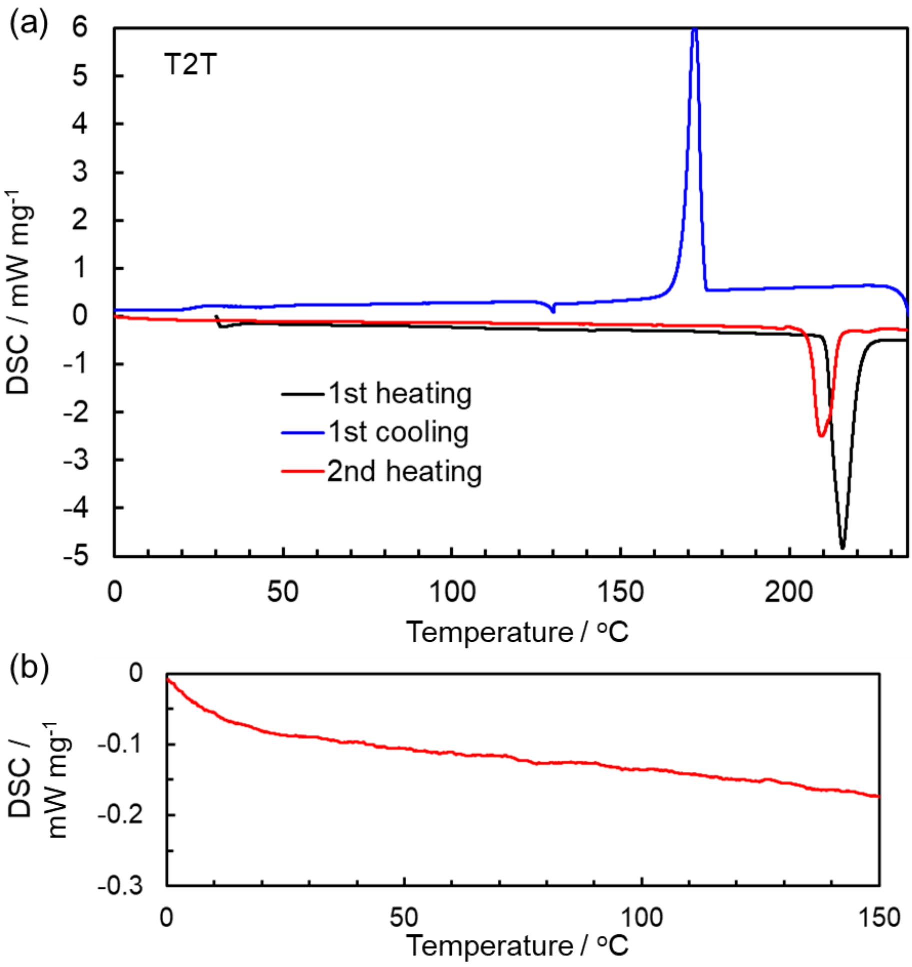

Fig. S23 (a) DSC curves of **T2T** by heating and cooling processes. (b) Focusing T_g signal at 2nd heating.

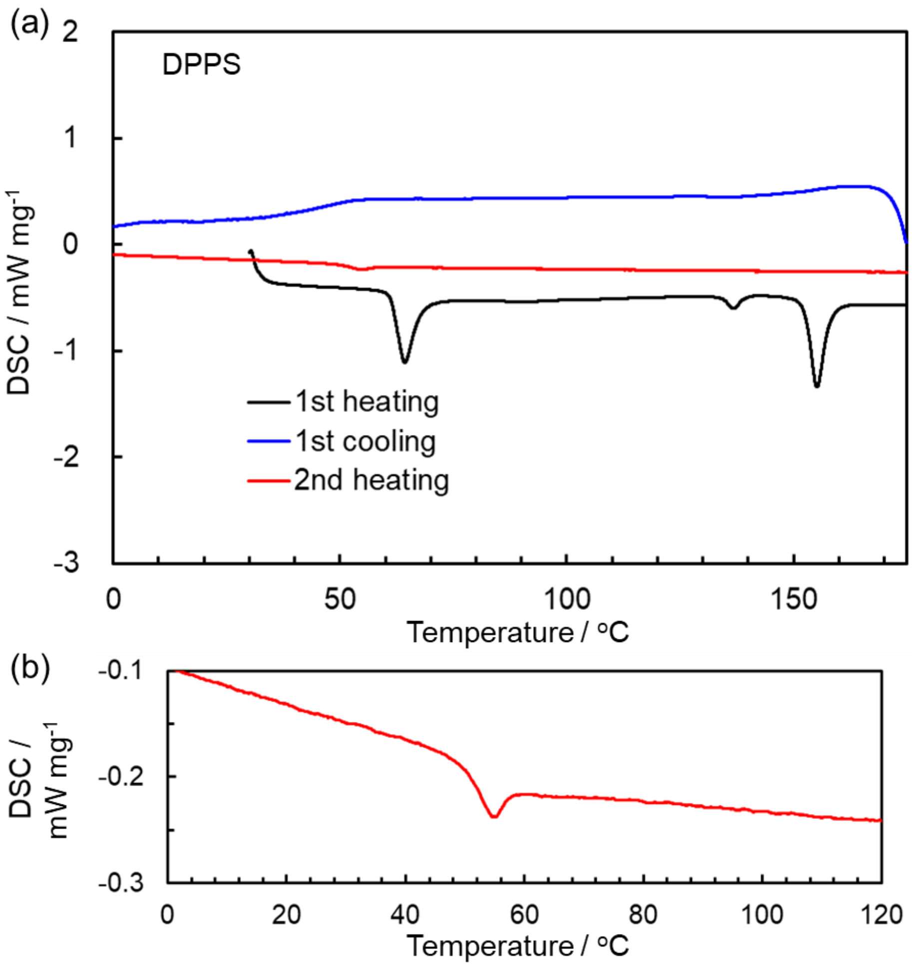

Fig. S24 (a) DSC curves of **DPPS** by heating and cooling processes. (b) Focusing T_g signal at 2nd heating.

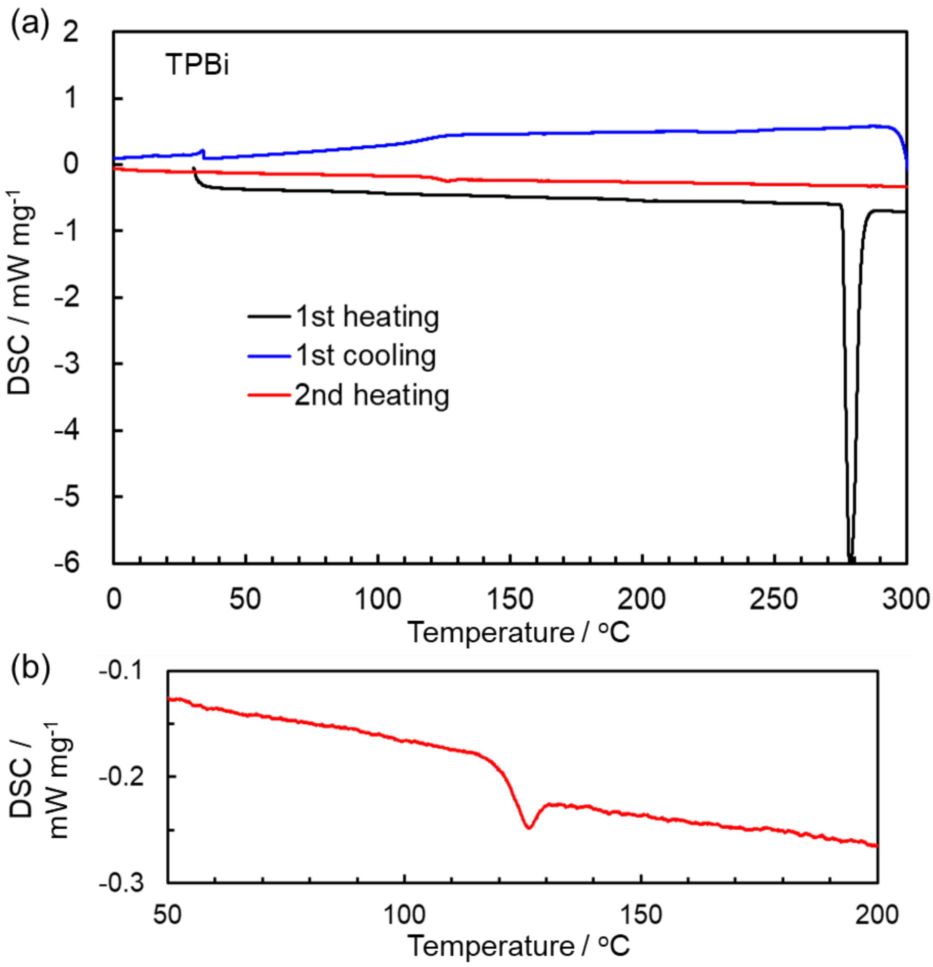

Fig. S25 (a) DSC curves of **TPBi** by heating and cooling processes. (b) Focusing T_g signal at 2nd heating.

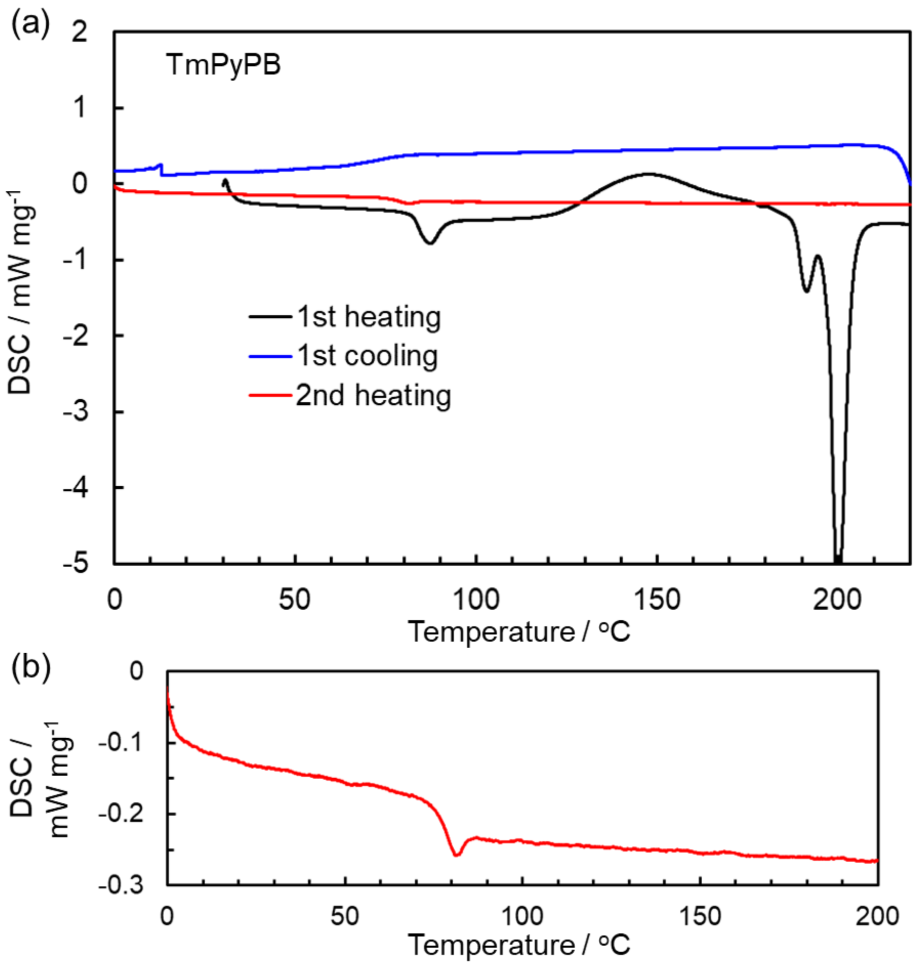

Fig. S26 (a) DSC curves of **TmPyPB** by heating and cooling processes. (b) Focusing T_g signal at 2nd heating.

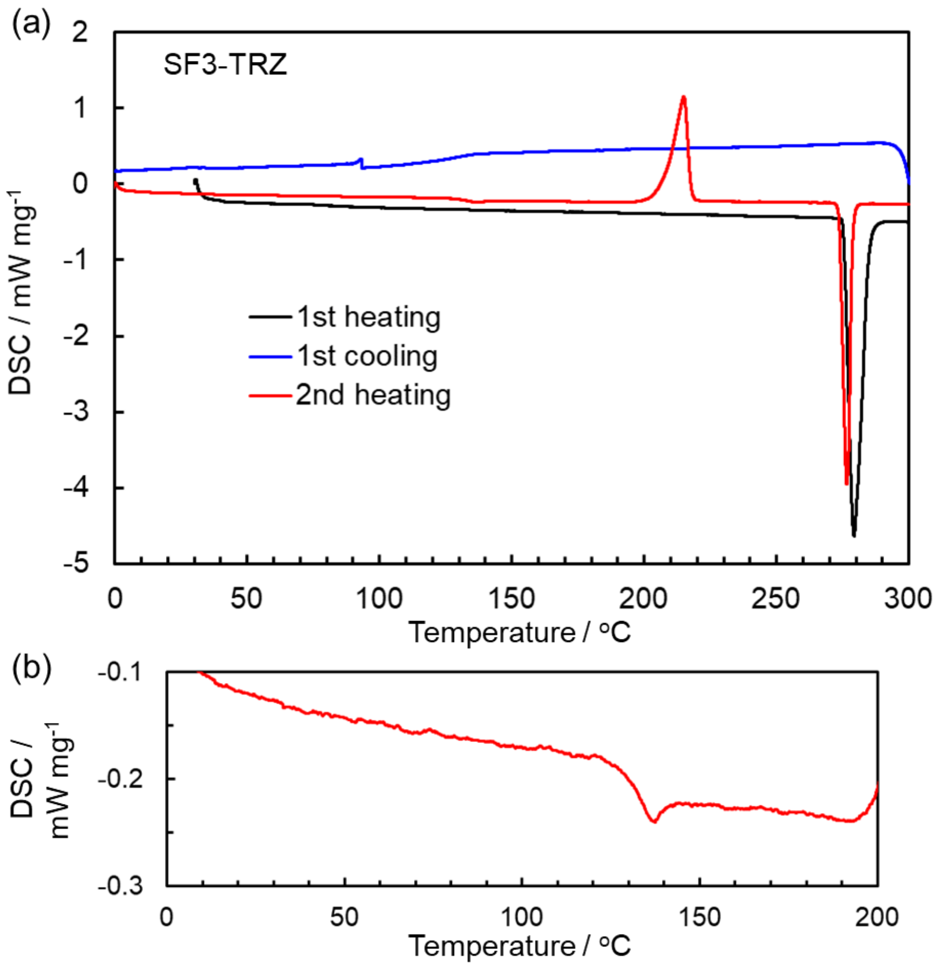

Figure S27. (a) DSC curves of **SF3-TRZ** by heating and cooling processes. (b) Focusing T_g signal at 2nd heating.

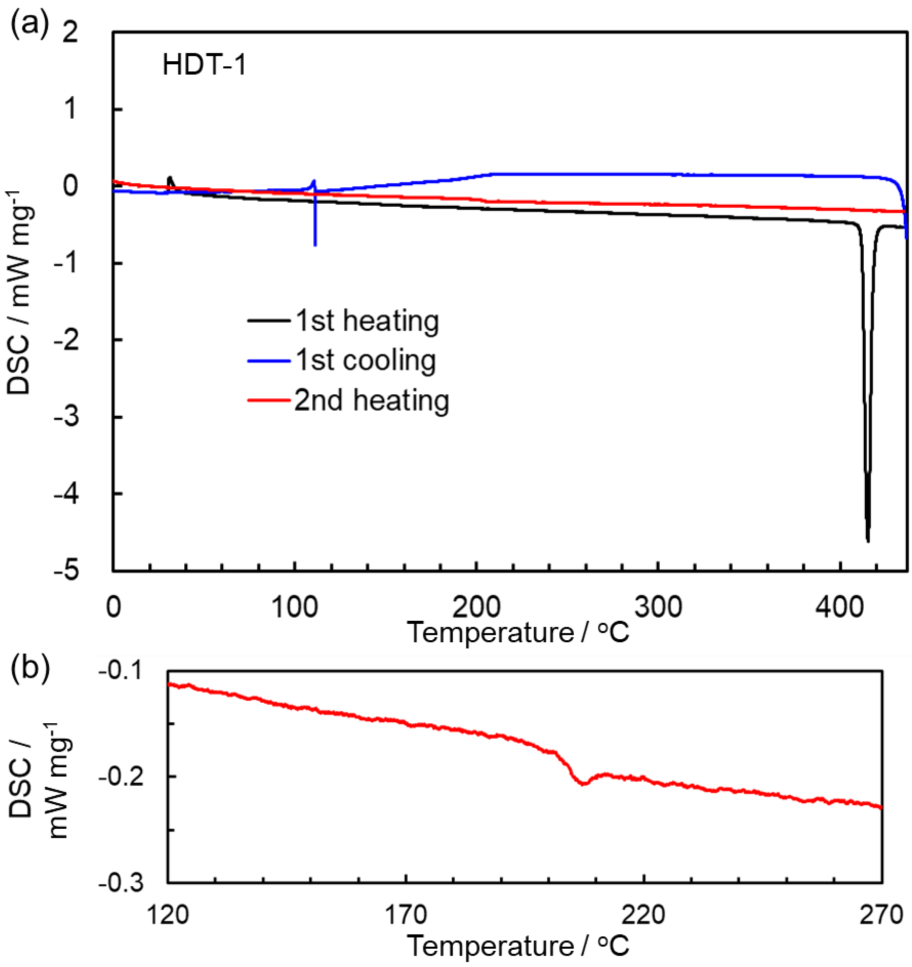

Fig. S28 (a) DSC curves of **HDT-1** by heating and cooling processes. (b) Focusing T_g signal at 2nd heating.

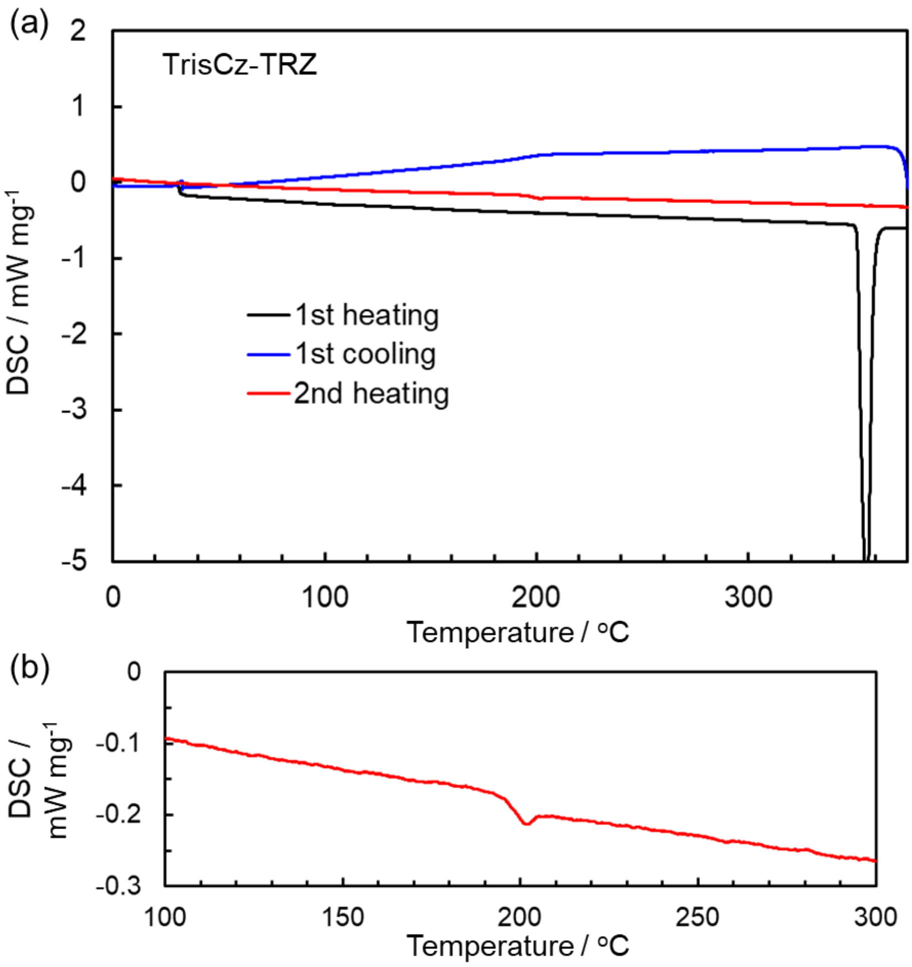

Fig. S29 (a) DSC curves of **TrisCz-TRZ** by heating and cooling processes. (b) Focusing T_g signal at 2[nd] heating.

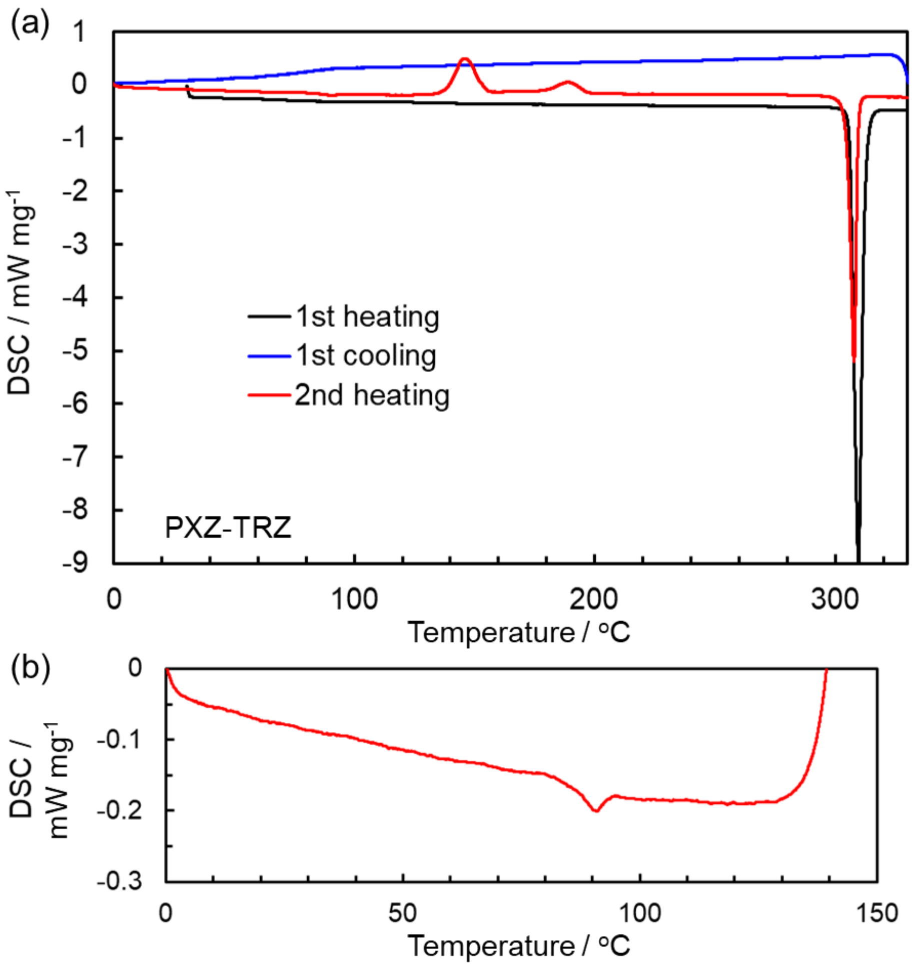

Fig. S30 (a) DSC curves of **PXZ-TRZ** by heating and cooling processes. (b) Focusing T_g signal at 2nd heating.

13. Appendix: Characterization of DSC curves

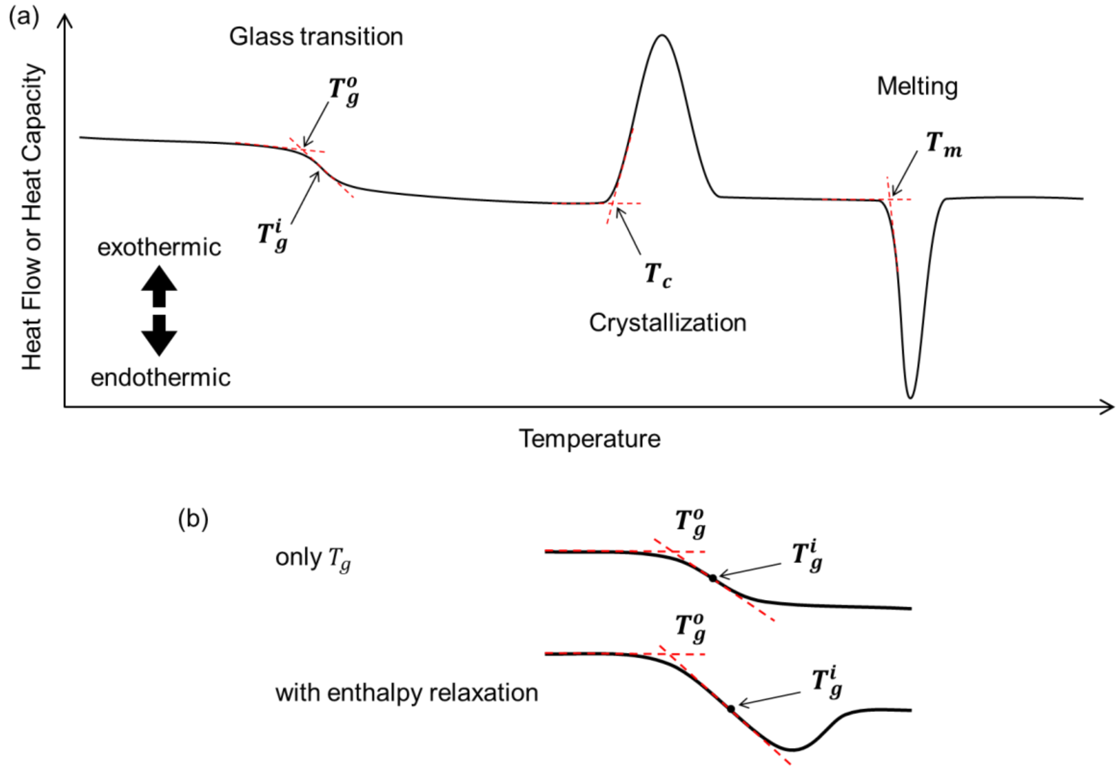

Fig. S31 (a) Illustration of typical DSC curves and definition of T_g^o, T_g^i, T_c, and T_m. (b) Focusing illustration of glass transition temperature region in case of with and without enthalpy relaxation.

14. Appendix: Purity of materials

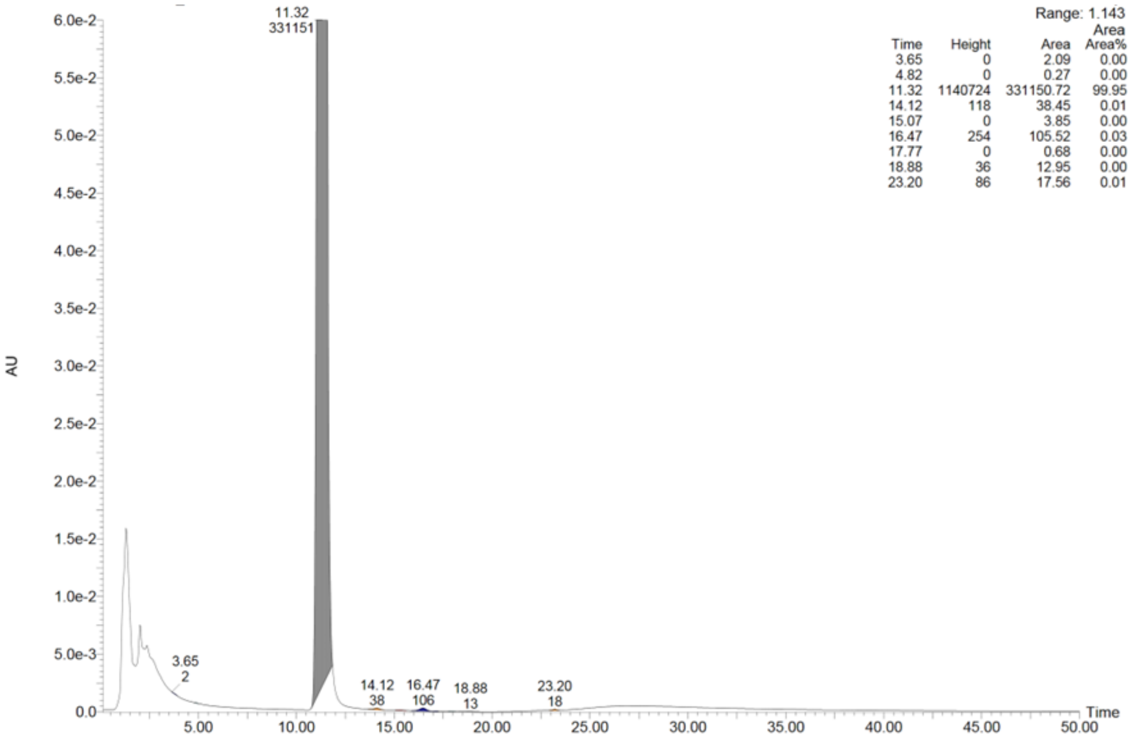

Fig. S32 HPLC analytical chart for **mCP**.

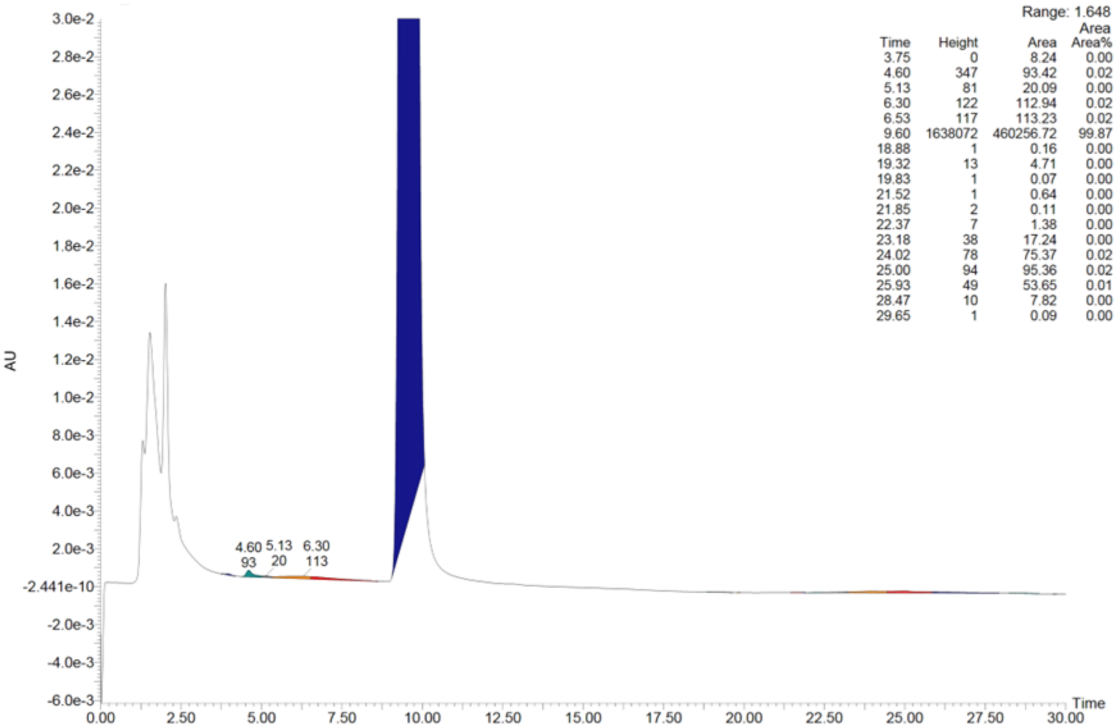

Fig. S33 HPLC analytical chart for CBP.

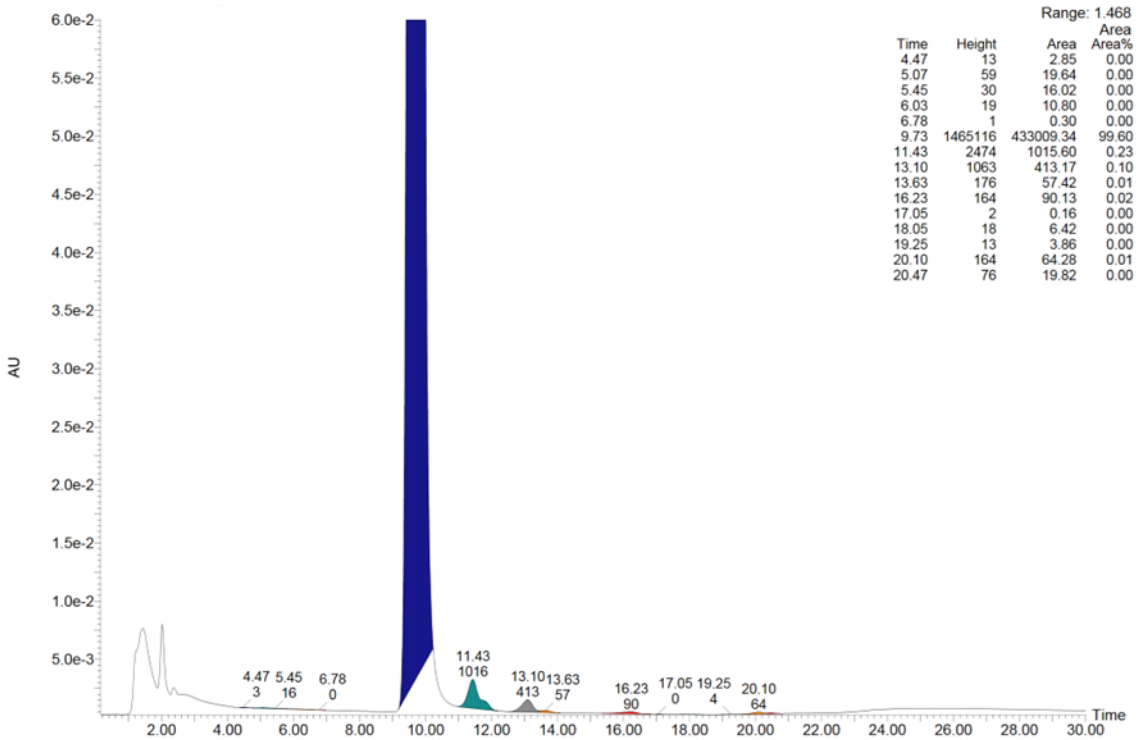

Fig. S34 HPLC analytical chart for **CBP**.

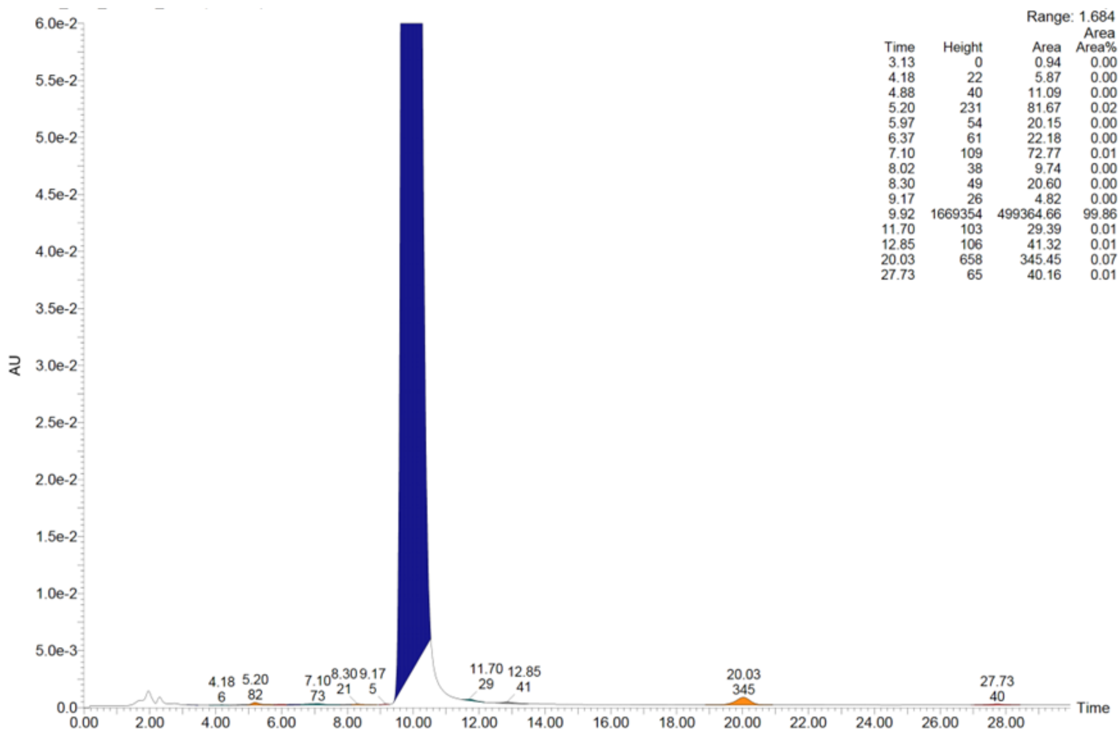

Fig. S35 HPLC analytical chart for **Cz-TRZ**.

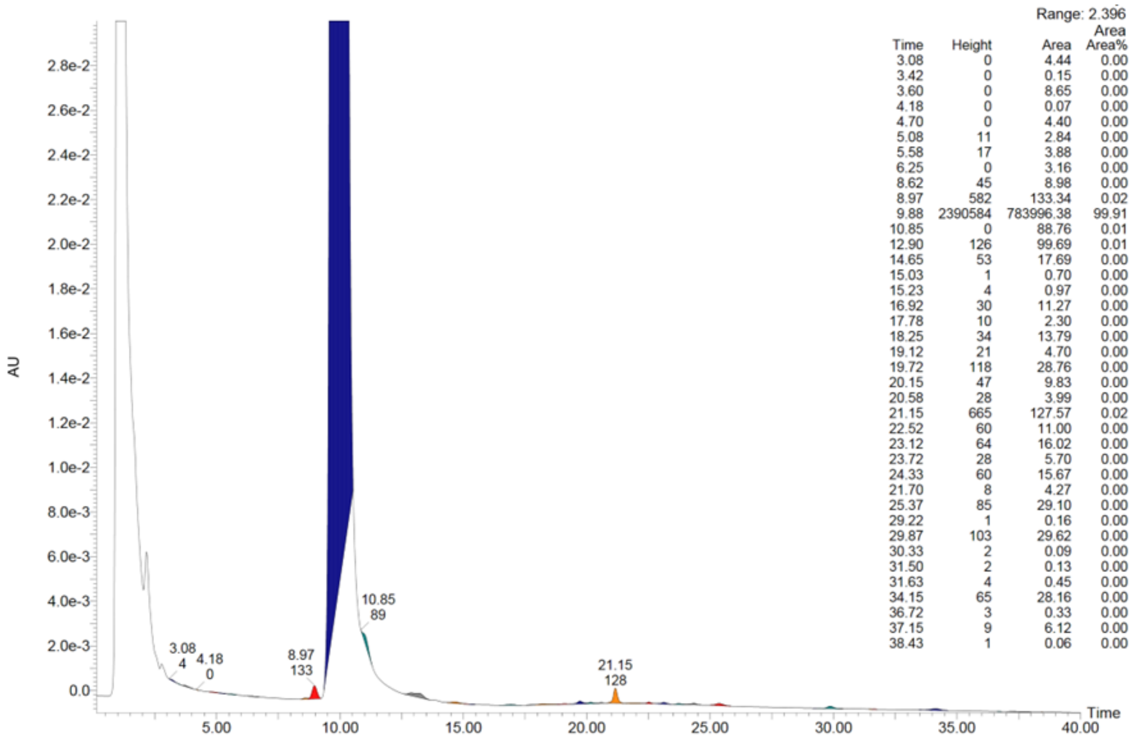

Time	Height	Area	Area Area%
3.08	0	4.44	0.00
3.42	0	0.15	0.00
3.60	0	8.65	0.00
4.18	0	0.07	0.00
4.70	0	4.40	0.00
5.08	11	2.84	0.00
5.58	17	3.88	0.00
6.25	0	3.16	0.00
8.62	45	8.98	0.00
8.97	582	133.34	0.02
9.88	2390584	783996.38	99.91
10.85	0	88.76	0.01
12.90	126	99.69	0.01
14.65	53	17.69	0.00
15.03	1	0.70	0.00
15.23	4	0.97	0.00
16.92	30	11.27	0.00
17.78	10	2.30	0.00
18.25	34	13.79	0.00
19.12	21	4.70	0.00
19.72	118	28.76	0.00
20.15	47	9.83	0.00
20.58	28	3.99	0.00
21.15	665	127.57	0.02
22.52	60	11.00	0.00
23.12	64	16.02	0.00
23.72	28	5.70	0.00
24.33	60	15.67	0.00
21.70	8	4.27	0.00
25.37	85	29.10	0.00
29.22	1	0.16	0.00
29.87	103	29.62	0.00
30.33	2	0.09	0.00
31.50	2	0.13	0.00
31.63	4	0.45	0.00
34.15	65	28.16	0.00
36.72	3	0.33	0.00
37.15	9	6.12	0.00
38.43	1	0.06	0.00

Fig. S36 HPLC analytical chart for **PPT**.

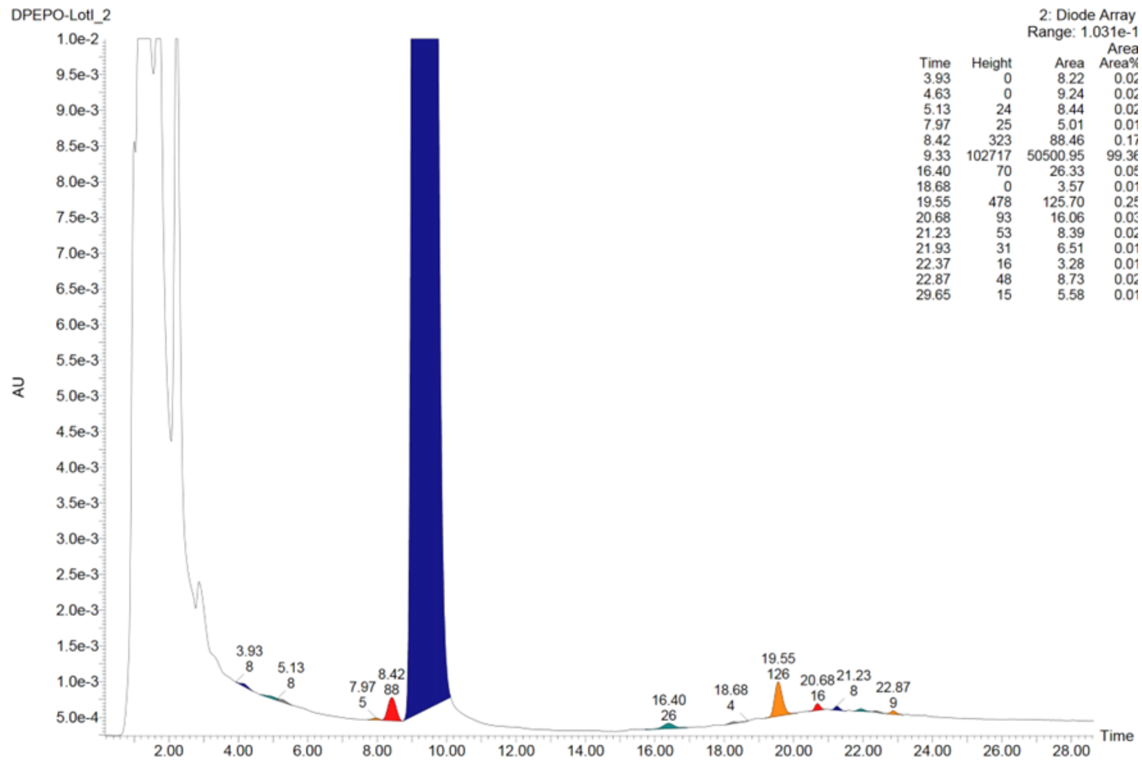

Time	Height	Area	Area Area%
3.93	0	8.22	0.02
4.63	0	9.24	0.02
5.13	24	8.44	0.02
7.97	25	5.01	0.01
8.42	323	88.46	0.17
9.33	102717	50500.95	99.36
16.40	70	26.33	0.05
18.68	0	3.57	0.01
19.55	478	125.70	0.25
20.68	93	16.06	0.03
21.23	53	8.39	0.02
21.93	31	6.51	0.01
22.37	16	3.28	0.01
22.87	48	8.73	0.02
29.65	15	5.58	0.01

Fig. S37 HPLC analytical chart for **DPEPO**.

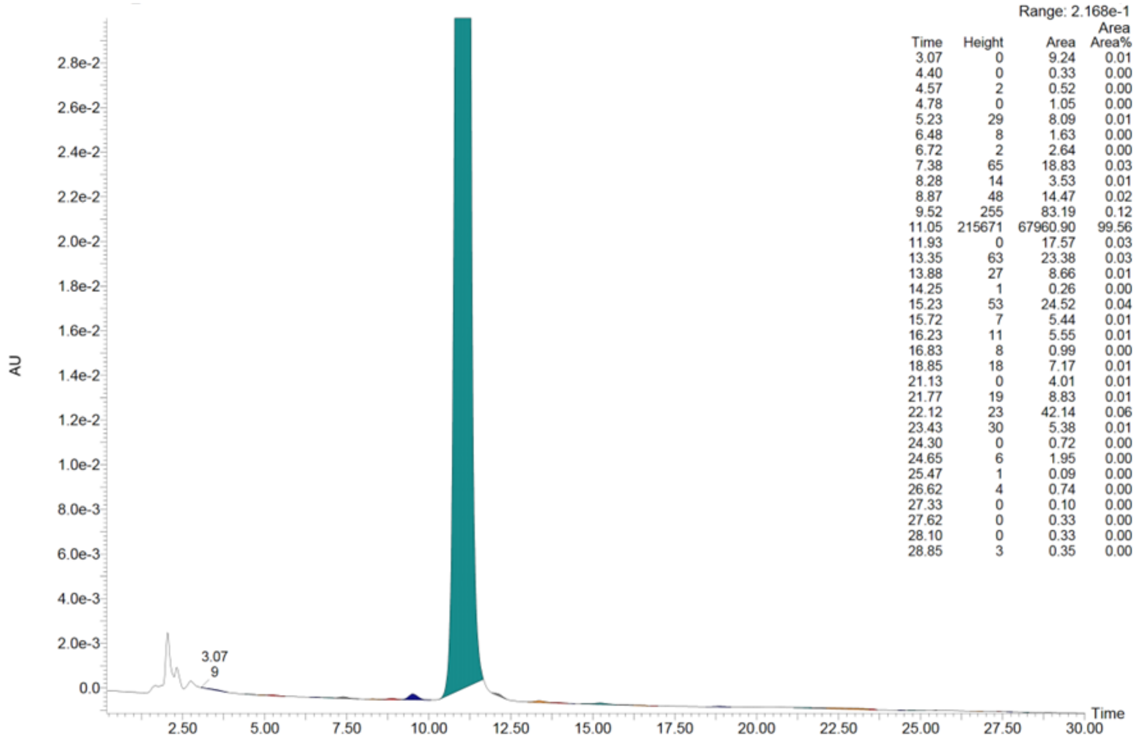

Fig. S38 HPLC analytical chart for **TAPC**.

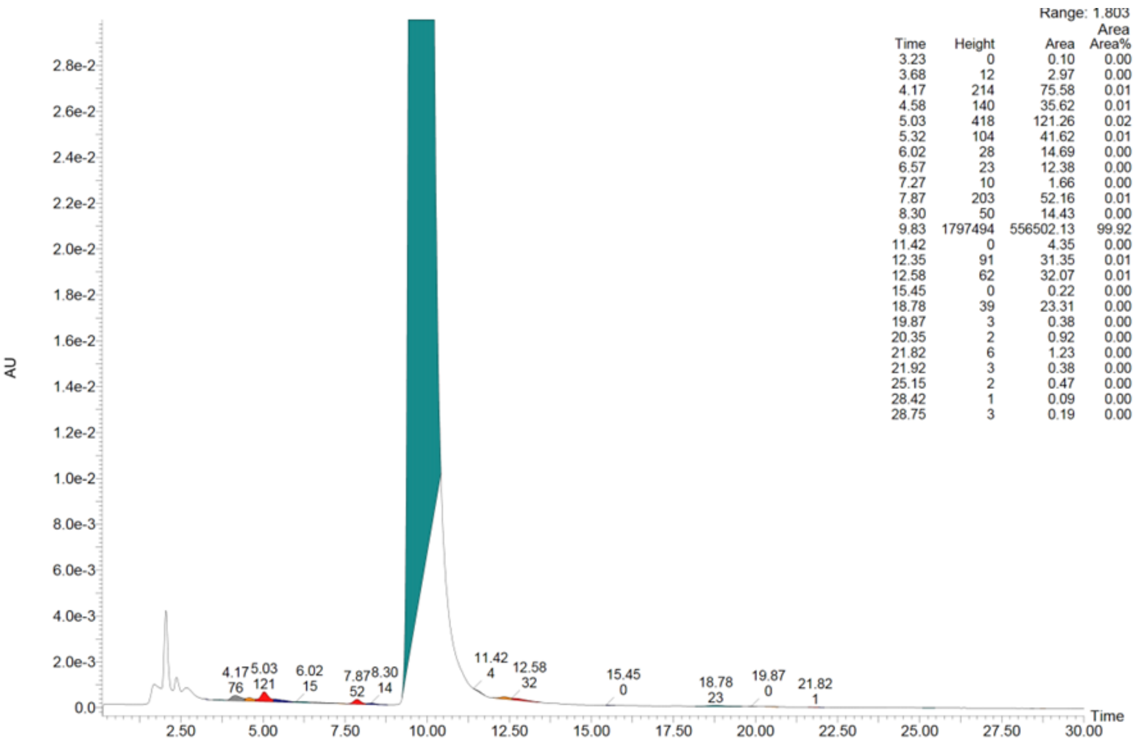

Fig. S39 HPLC analytical chart for **Tris-PCz**.

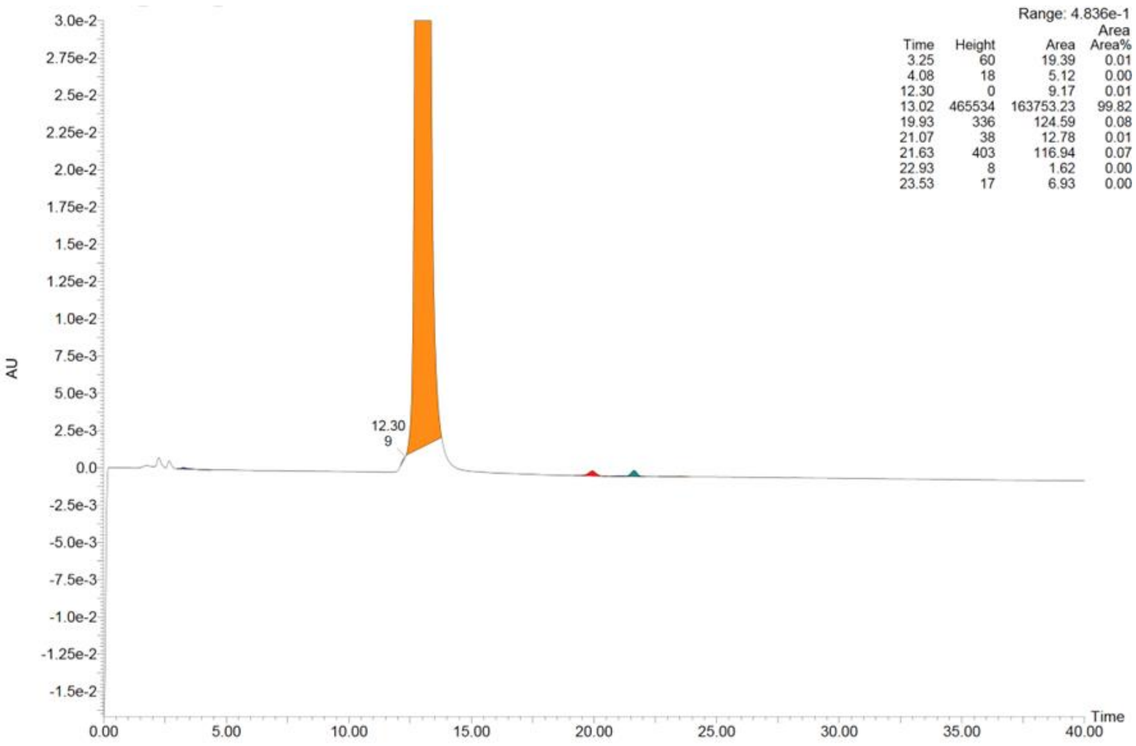

Fig. S40 HPLC analytical chart for **α-NPD**.

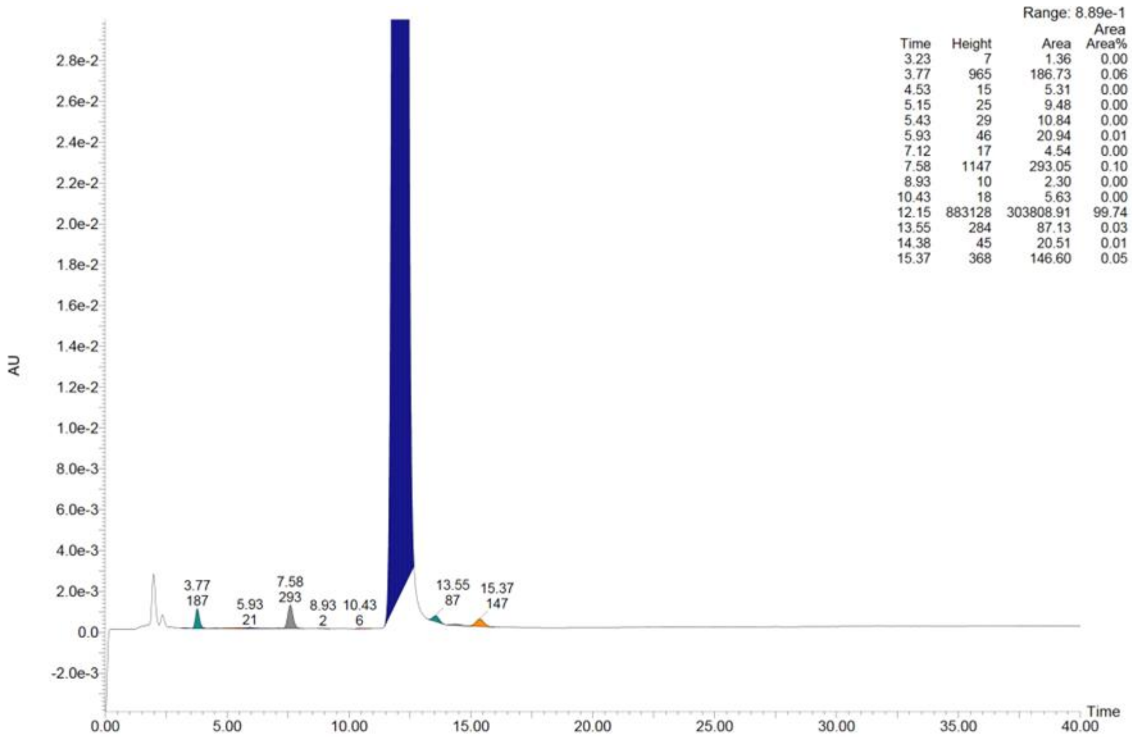

Fig. S41 HPLC analytical chart for **TCTA**.

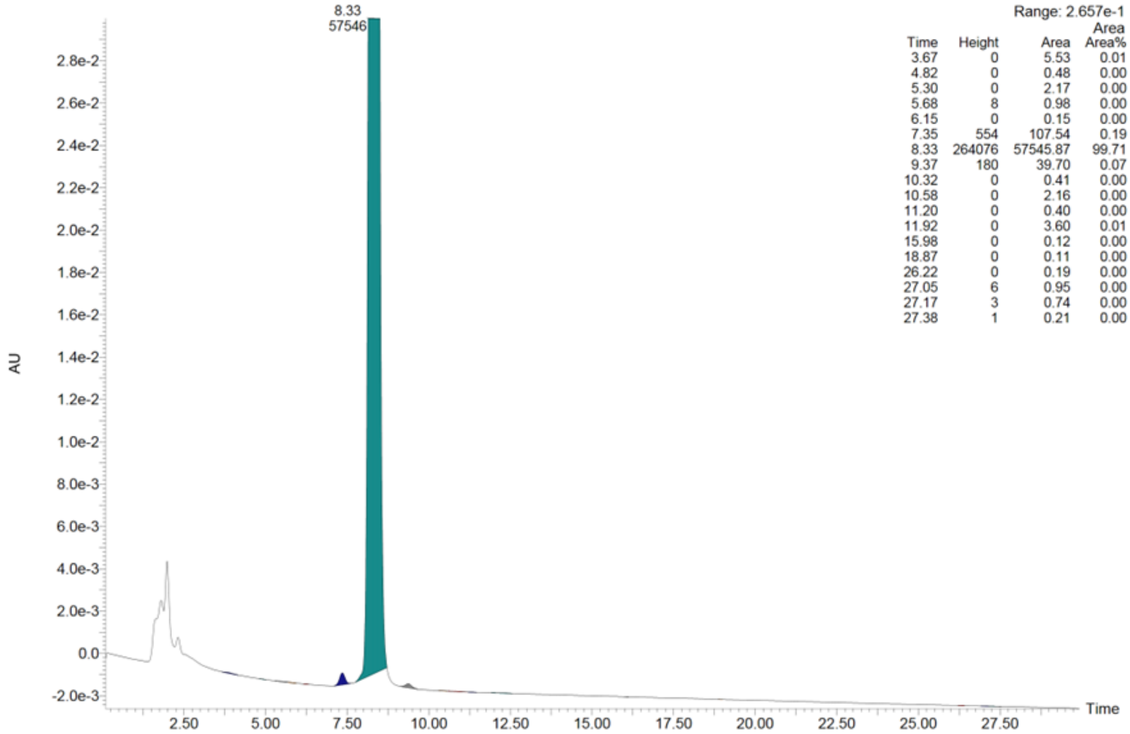

Fig. S42 HPLC analytical chart for **TPD**.

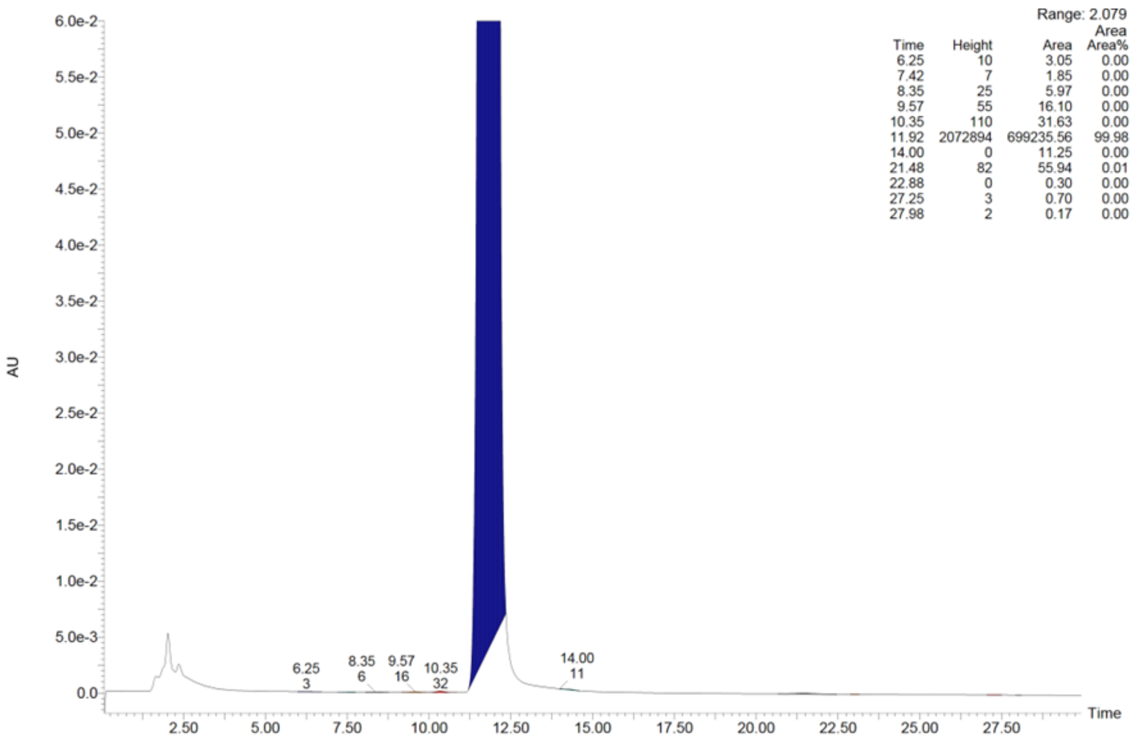

Fig. S43 HPLC analytical chart for **T2T**.

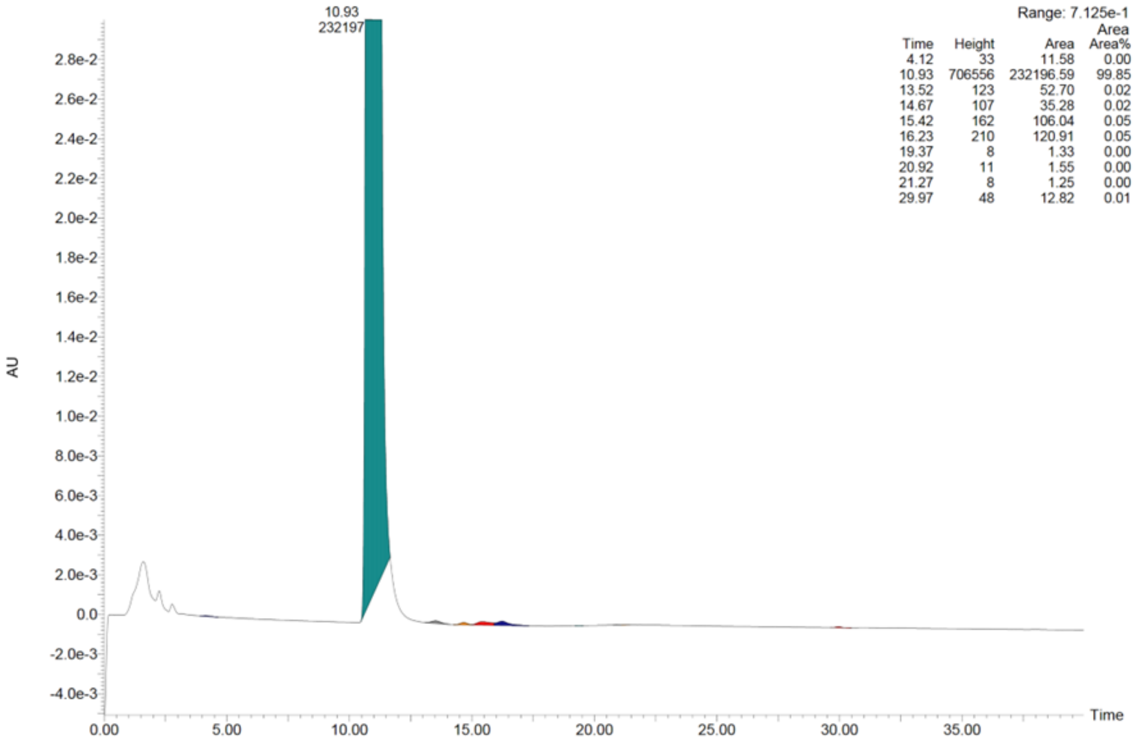

Fig. S44 HPLC analytical chart for **TPBi**.

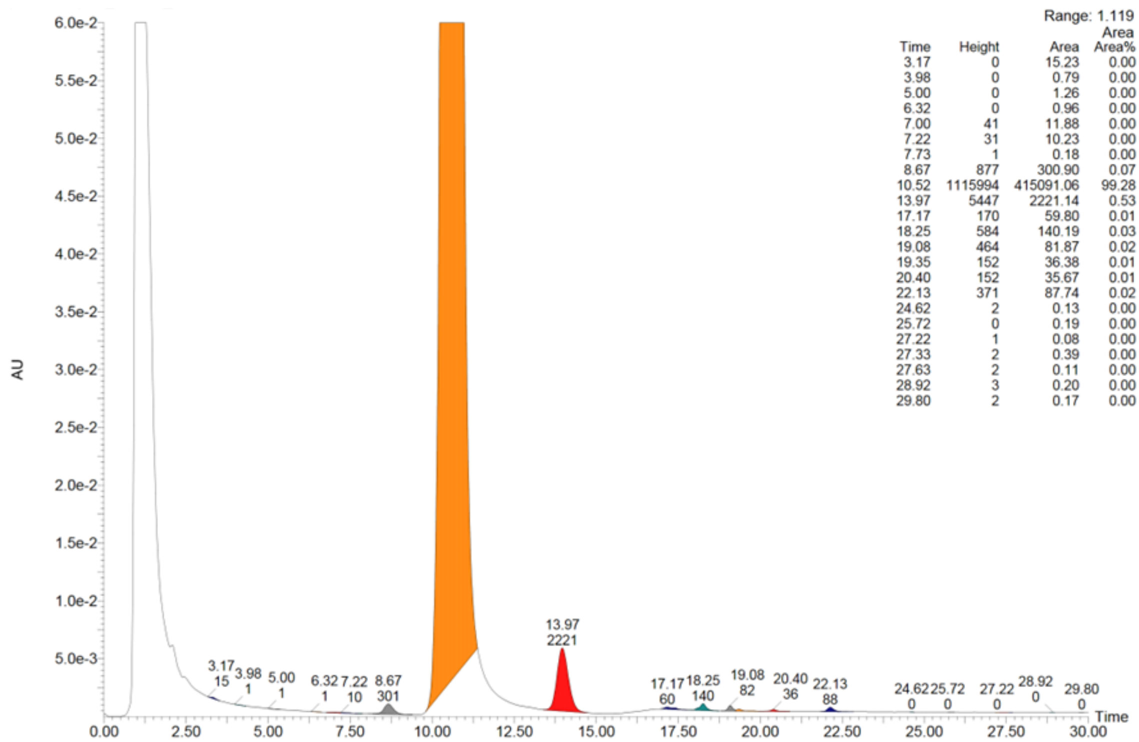

Fig. S45 HPLC analytical chart for **TmPyPB**.

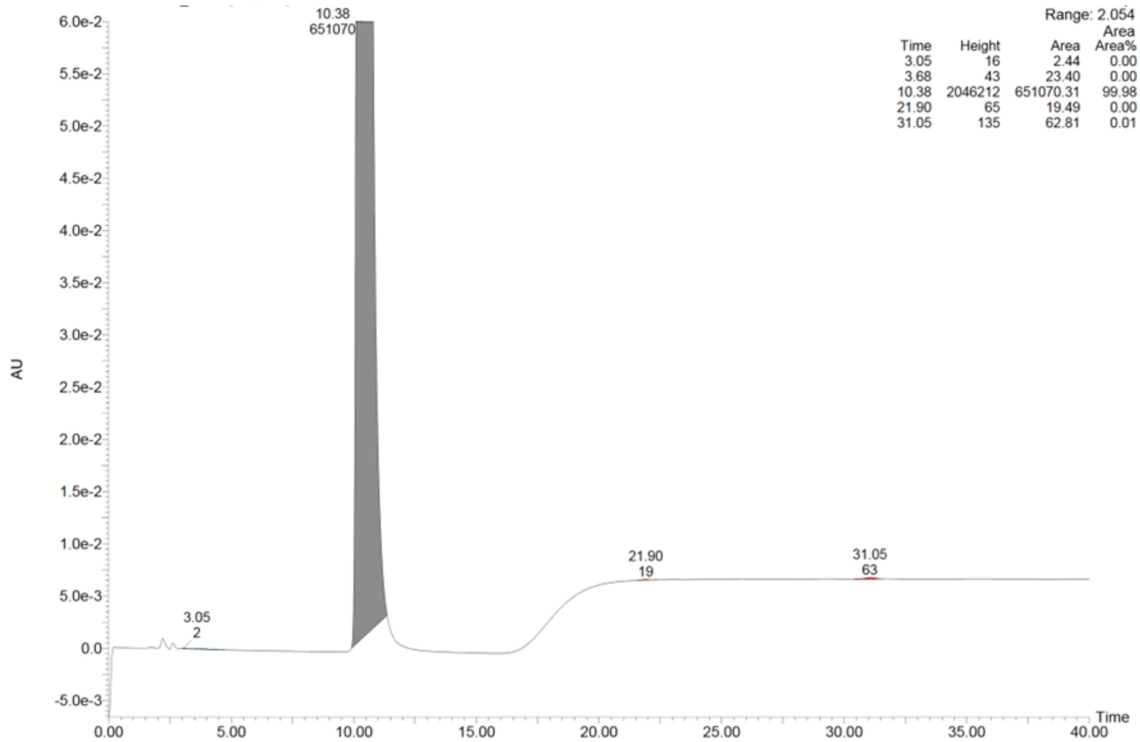

Fig. S46 HPLC analytical chart for **SF3-TRZ**.

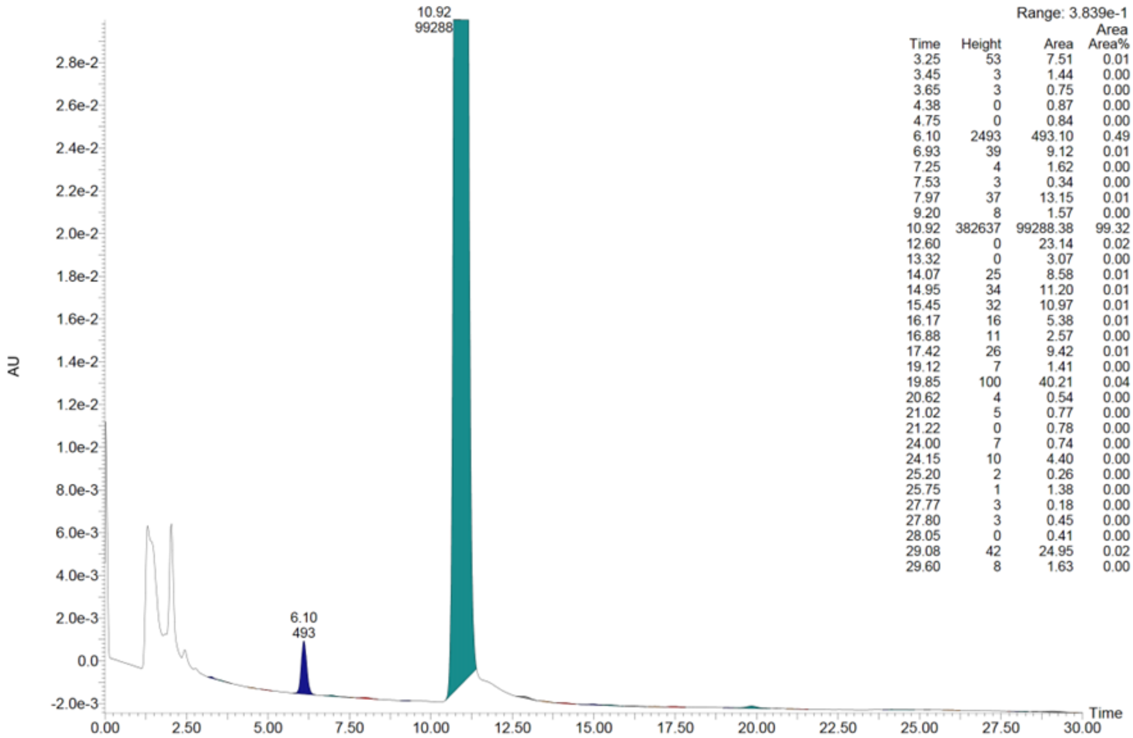

Fig. S47 HPLC analytical chart for **4CzIPN**.

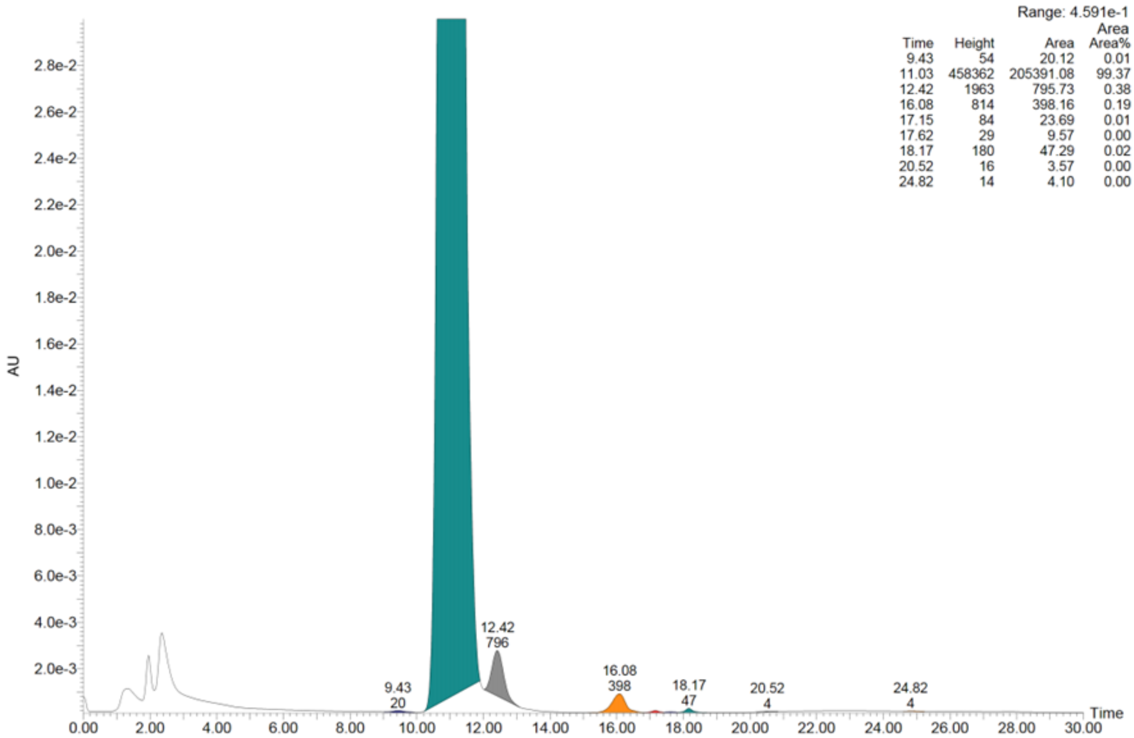

Fig. S48 HPLC analytical chart for **5CzTRZ**.

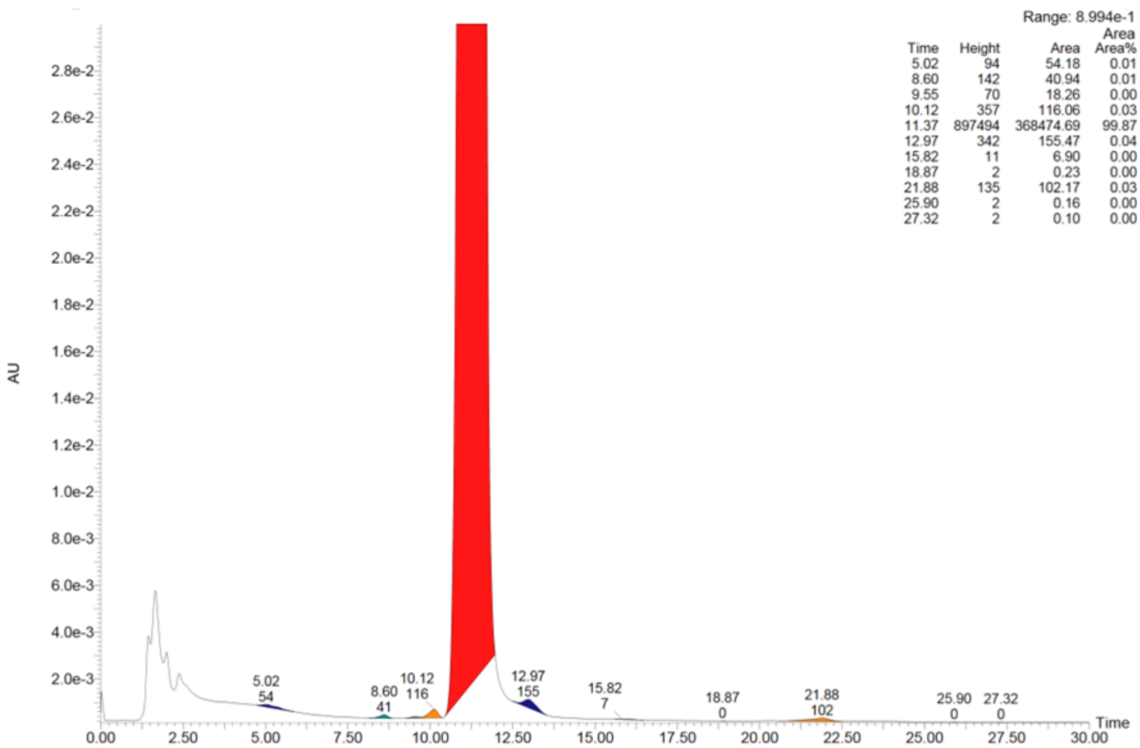

Fig. S49 HPLC analytical chart for **HDT-1**.

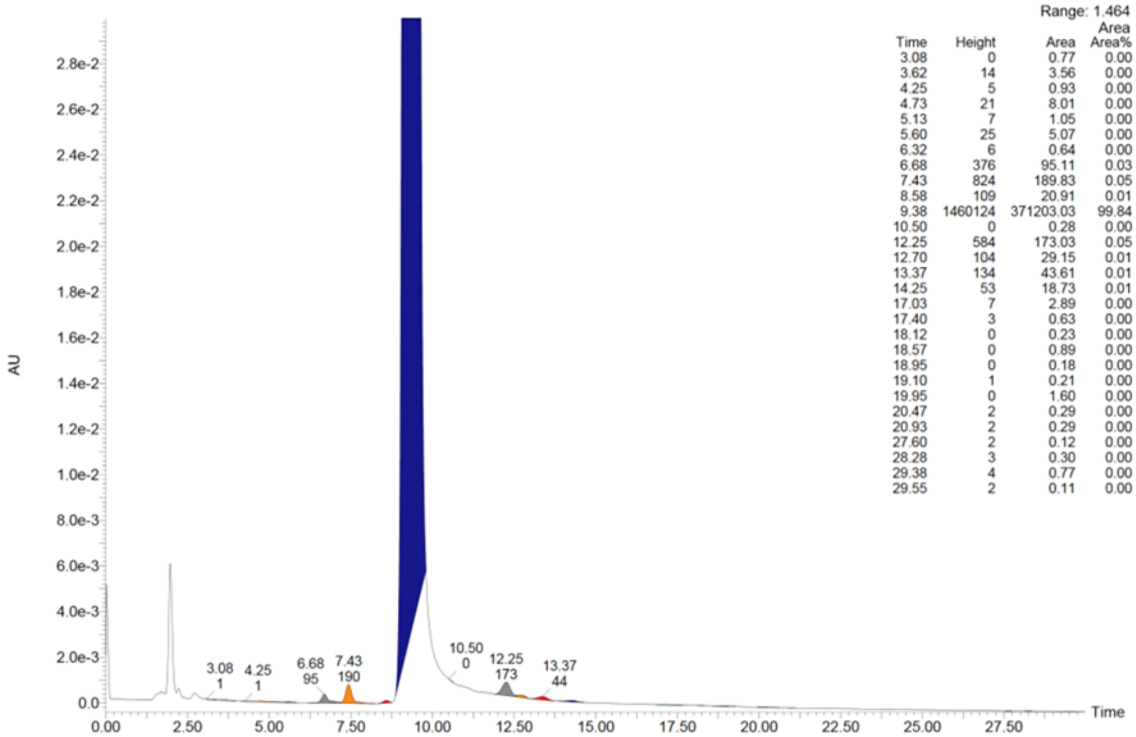

Fig. S50 PLC analytical chart for **TrisCz-TRZ**.

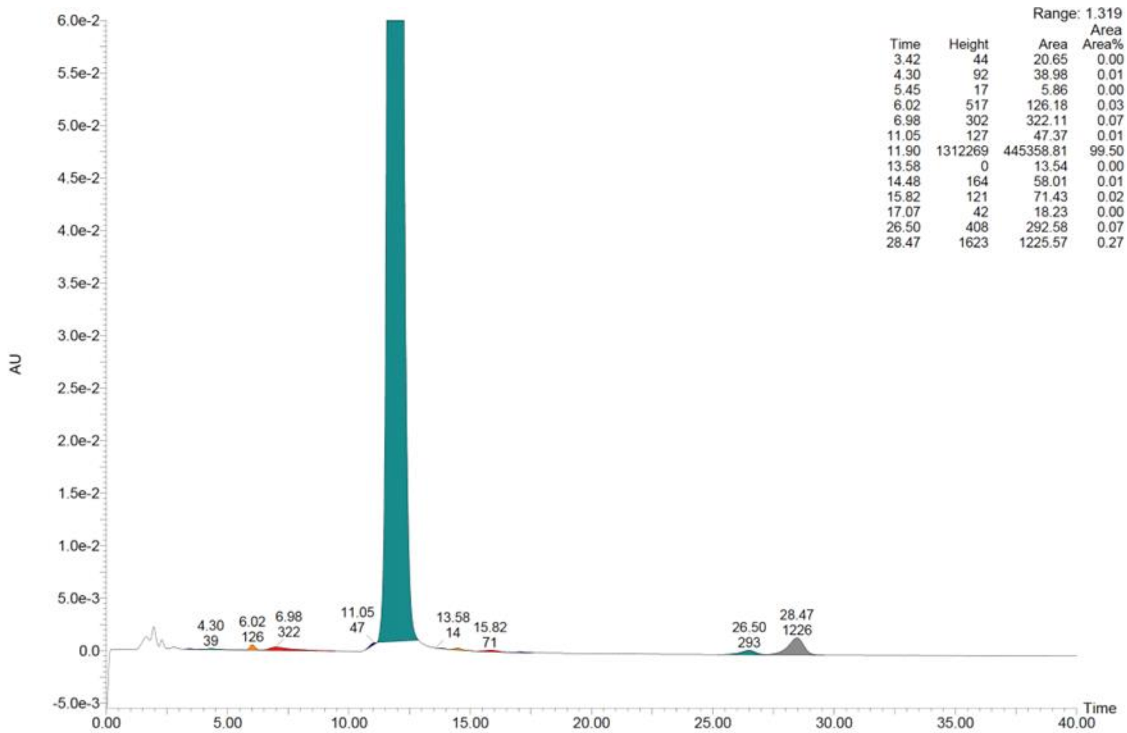

Fig. S51 HPLC analytical chart for **PXZ-TRZ**.